Loss of host tissue transglutaminase boosts antitumor T cell immunity by altering STAT1/STAT3 phosphorylation in ovarian cancer

Livia Elena Sima [1,2] Siqi Chen,[3] Horacio Cardenas,[1] Guangyuan Zhao [1] Yinu Wang,[1] Cristina Ivan,[4] Hao Huang,[1] Bin Zhang,[3,5] Daniela Matei[1,5,6]

ABSTRACT

Background Tissue transglutaminase (TG2), an enzyme overexpressed in cancer cells, promotes metastasis and resistance to chemotherapy. Its distinct effects in cancer versus the host compartments have not been elucidated.
Methods Here, by using a TG2$^{-/-}$ syngeneic ovarian cancer mouse model, we assessed the effects of TG2 deficiency in the host tissues on antitumor immunity and tumor progression. Multicolor flow cytometry was used to phenotype immune cell populations in the peritoneal environment. Cancer cells recovered from malignant ascites were characterized by RNA sequencing, proliferation, and apoptosis assays.
Results We observed that host TG2 loss delayed tumor growth and ascites accumulation and caused increased infiltration of CD8$^+$ T cells and decreased numbers of myeloid cells in the peritoneal fluid. Tumor antigen-specific CD8$^+$ T cell cytotoxic responses were enhanced in ascites from TG2$^{-/-}$ versus TG2$^{+/+}$ mice and CD8$^+$ T cell depletion caused accelerated ascites accumulation in TG2$^{-/-}$ mice. CD8$^+$ T cells from tumor-bearing TG2$^{-/-}$ mice displayed an effector T cell phenotype, differentiated toward effector memory (T$_{em}$). Mechanistically, absence of TG2 augmented signals promoting T cell activation, such as increased cytokine-induced STAT1 and attenuated STAT3 phosphorylation in T cells. Additionally, immune-suppressive myeloid cell populations were reduced in the peritoneal milieu of TG2$^{-/-}$ tumor-bearing mice. In response to the more robust immune response caused by loss of TG2, cancer cells growing intraperitoneally exhibited an interferon-γ (IFN-γ) responsive gene signature and underwent apoptosis. In human specimens, stromal, not tumor, TG2 expression correlated indirectly with numbers of tumor-infiltrating lymphocytes.
Conclusions Collectively, our data demonstrate decreased tumor burden, increased activation and effector function of T cells, and loss of immunosuppressive signals in the tumor microenvironment of TG2$^{-/-}$ mice. We propose that TG2 acts as an attenuator of antitumor T cell immunity and is a new immunomodulatory target.

BACKGROUND

Tissue transglutaminase (TG2) belongs to the transglutaminase family and contains an N-terminus β-sandwich domain, which binds to fibronectin, a catalytic triad C^{277}H^{335}D^{358}, which carries out the acyl-transfer function, and two β-barrel domains.[1 2] A GTP/GDP binding site is located between the catalytic and the first barrel domain. The functions of the protein are modulated through large allosteric changes, which are tightly regulated by Ca^{2+} and GTP levels.[3] Over the past decade, several studies have linked TG2 to cancer. Upregulation of TG2 was reported in ovarian,[4 5] pancreatic carcinoma,[6] glioblastoma,[7] lung,[8] and breast cancer.[9] TG2 overexpression was correlated with poor clinical outcome in pancreatic,[10] ovarian,[11] and lung cancer,[12] suggesting that it functioned as a tumor promoter, and several oncogenic pathways (NF-κB, β-catenin, Rho, FAK, Akt, YAP) were shown to be activated by TG2 and linked to cancer progression.[13–17] TG2 expression was linked to chemotherapy and radiation resistance in cancer cells.[18] This was attributed to activation of the NF-κB survival pathway[19 20] and of 'outside-in' signaling.[10] Second, TG2 was linked to metastasis in ovarian,[4 5] breast, and lung cancer models.[16 21] Third, TG2 was found to be highly expressed in cancer stem cells in ovarian,[22] breast,[15] skin,[23] and brain cancer models.[24] While the majority of the evidence points to an oncogenic phenotype linked to TG2, there is still lack of consensus regarding which function(s) of the protein promote cancer progression, with evidence pointing to context-dependent roles of TG2.

Studies linking TG2 to cancer progression have focused on the activity of TG2 expressed in cancer cells, while the functions of the protein expressed by the host have been less well investigated. Given TG2's wide pattern of expression, it is reasonable to hypothesize that its expression in normal tissues could also influence cancer initiation

and/or progression. TG2 is expressed by fibroblasts, endothelium, and immune cells, which are components of the tumor microenvironment (TME) and of the metastatic niche. T and B lymphocytes, myeloid cells, and macrophages express variable amounts of TG2, and the enzyme was shown to alter immune responses under physiological and pathological conditions. TG2 null mice were shown to display mildly increased autoimmunity with aging[25] and were more efficient in clearing *Mycobacterium tuberculosis.*[26] TG2 mediates the interaction between dendritic cells and T cells promoting responses to antigen stimulation,[27] while TG2^{-/-} T cells were shown to generate decreased numbers of memory T cells.[28] On the other hand, TG2 null macrophages were less efficient in phagocytosis[29 30] and displayed a proinflammatory phenotype, characterized by interleukin-6 (IL-6) and tumor necrosis factor-α (TNF-α) secretion.[31] However, the role of TG2 in antitumor immunity has not been studied.

Here, by using the ID8 syngeneic ovarian cancer (OC) model, we report the effects of host TG2 deficiency on peritoneal tumor progression and antitumor immune responses. We show that OC dissemination was delayed and ascites formation was inhibited in TG2^{-/-} mice. The peritoneal environment of TG2^{-/-} mice was enriched in cytotoxic CD8^{+} T cells and T cells differentiated to an effector/memory phenotype. STAT3 activation in response to IFN-γ, IL-6 and TGF-β was decreased in TG2^{-/-} CD4^{+} and CD8^{+} T cells, consistent with an immunostimulated phenotype. On the other hand, proliferation of cancer cells was inhibited by treatment with ascites from TG2^{-/-} compared with TG2^{+/+} mice and cancer cells isolated from TG2^{-/-} ascites exhibited improved antigen presentation. Our data support that loss of TG2 in the host promotes an antitumor cytotoxic T cell response, limiting disease progression.

MATERIALS AND METHODS
Animals
Female C57BL/6 mice (6–8 weeks of age) were purchased from Envigo (Indianapolis, Indiana, USA). TG2 knockout mice (TG2-KO) were generated by Nanda *et al.*[32] A TG2-KO mice colony was established at Northwestern University using breeders provided by Dr Gail Johnson, University of Rochester. TG2 knockout was verified by PCR-based genotyping using tail gDNA and the primers described in online supplemental table S1. In addition, absence of TG2 protein was confirmed in liver tissue by western blotting. Representative genotyping results are presented in online supplemental figure 1A and B. Mice were housed in a specific pathogen-free facility, and all studies were carried out under Animal Use Protocol #IS00002537 approved by the Northwestern University Animal Care and Use Committees and performed in accordance with federal regulations.

Cell lines
Murine ID8 OC cells were provided by Dr Katherine Roby (University of Kansas). ID8 ovalbumin-GFP-expressing cells (ID8-OVA) were produced by transducing ID8 cells with MIGR1-ovalbumin (OVA)-IRES-eGFP vector and selected by fluorescence activated cell sorting (FACS) based on green fluorescence protein (GFP) expression (PMC2883609). OVA production by ID8 cells was confirmed by ELISA. ID8 and ID8-OVA cells were grown in Dulbecco Modified Eagle Medium (DMEM, Corning, Cat. # 10-017-CV, Manassas, Virginia, USA) supplemented with 10% fetal bovine serum (FBS) and 1% penicillin/streptomycin solution.

In vivo experiments
Female TG2-KO and wild-type C57BL/6 mice, 6–8 weeks old, were injected intraperitoneally with 5 million ID8 cells or ID8-OVA cells to induce tumors. Numbers of tumors >1 mm, volume and cellular content of abdominal ascites, and spleen weights were measured at necropsy, typically at 6–7 weeks after inoculation of ID8 cells. Spleens and ascites of mice implanted with ID8-OVA cells were used to isolate immune cell populations. For survival experiments, tumor development induced by ID8 cells was allowed to continue until mice showed accumulation of abdominal ascites and 15% increase or loss of body weight, body condition score of 2 (unconditioned, thin) or less, or signs of distress and significant lethargy.

Tissue processing
Spleens were mechanically dissociated and passed through a 70 µm strainer to produce single-cell suspensions. Red cells were lysed using RBC lysis buffer (BioLegend, Cat. #420301) for 3 min at room temperature (RT) followed by quenching with RPMI medium. After centrifugation, cells were resuspended in cell culture media and used for experiments. For all immune assays, cR10 media was used consisting of RPMI 1640 medium (Sigma-Aldrich, Cat. #R8758) supplemented with 10% FBS, penicillin/streptomycin solution, 1% Na-pyruvate, and 1% Minimum Essential Media (MEM). Ascites specimens were centrifuged to separate fluid and cellular fractions, and red cells were eliminated through lysis.

T cell assays
Ex vivo restimulation assay
Ex vivo restimulation assay was performed as described previously.[33] For IFN-γ and granzyme B secretion analyses, cells were rested for 3–5 hours in cR10 medium and then treated for 3 hours with phorbol 12-myristate 13-acetate (PMA, 50 ng/mL, Sigma Cat. # P8139), ionomycin (5 µg/mL, Fisher Scientific, Cat. # I24222), and brefeldin A (1:500, BioLegend, Cat. # 42060) in a 37°C incubator. Cells were stained for 15 min at 4°C with antibodies to surface antigens, fixed using BD Cytofix buffer (BD Biosciences, Fixation/Permeabilization Solution Kit, Cat. # 554714) for 15 min at 4°C, washed with BD Cytoperm buffer, and then stained in Perm/Wash buffer.
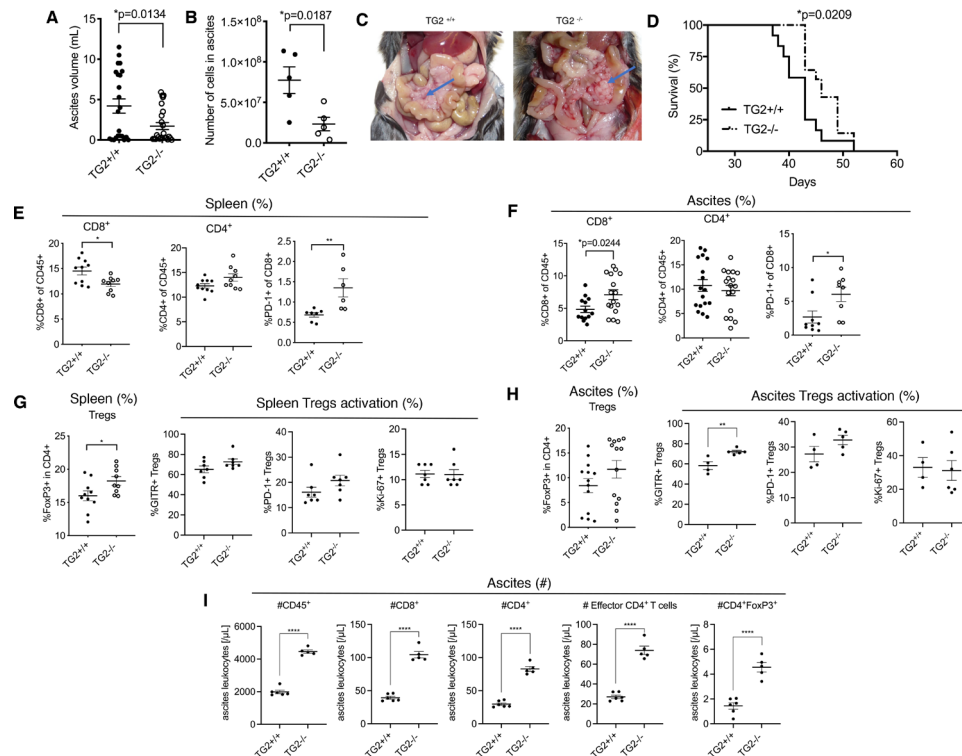
Figure 1 Tissue transglutaminase (TG2) promotes peritoneal tumor growth in a syngeneic ovarian cancer (OC) mouse model by preventing CD8⁺ T cell infiltration into ascites. (A, B) Volume of peritoneal ascites (mean±SEM, n=23 per group, cumulative data from four independent experiments are shown) (A), and numbers of cells in ascites (mean±SEM, n=5 per group, data from one representative experiment out of two performed are shown) (B) in C57BL/6 (TG2⁺/⁺) and TG2 knockout (TG2⁻/⁻) female mice 6 weeks after intraperitoneal injection of ID8 cells. Shown are t-test p values. (C) Images of peritoneal metastases in TG2⁺/⁺ and TG2⁻/⁻ abdominal cavities. Tumor implants are indicated by blue arrows. (D) Kaplan-Meier survival analysis of TG2⁺/⁺ (n=12) and TG2⁻/⁻ (n=14) mice injected intraperitoneally with ID8 cells. Graph represents data from one experiment out of two performed. (E–H) Measurements by flow cytometry of percentages of immune cells in TG2⁺/⁺ and TG2⁻/⁻ mice-bearing tumors induced by intraperitoneal inoculation of ID8 cells. (E) CD8⁺ and CD4⁺ T cells in spleens (TG2⁺/⁺, n=10; TG2⁻/⁻, n=9; data from two experiments). (F) CD8⁺ and CD4⁺ T cells in abdominal ascites (TG2⁺/⁺, n=13; TG2⁻/⁻, n=16; data from four experiments). (E, F) Programmed cell death protein 1 (PD-1) expressing CD8⁺ T cells in spleen (n=7 per group; data from one representative experiment) and ascites (n=9 per group; data pooled from three experiments). Values are means±SEM (*p<0.05; **p<0.01). (G, H) T regulatory cells (Tregs) in spleen (n=10 per group; data from two experiments) and ascites (n=13 per group; data from three experiments). Activation marker expressions from one representative experiment are shown (n=4–7 per group). (I) Absolute cell counts in ascites (TG2⁺/⁺, n=6; TG2⁻/⁻, n=5). Total cell counts were used for determination of total cell number for each subset from data retrieved from fluorescence activated cell sorting (FACS, ****p<0.0001).

In vitro T cell polarization

Splenocytes were obtained from non-tumor-bearing C57BL/6 and TG2-KO mice as described above. CD8⁺ and CD4⁺ T cells were obtained via magnetic bead separation using EasySep Mouse CD8a Positive Kit II (Stemcell Technology, Cat. # 18953) and EasySep Mouse CD4⁺ T Cell Isolation Kit (Stemcell Technologies, Cat. # 19852). Cells were counted using a Countess II (Life Technologies) instrument, seeded at 3×10⁵ cells/well in a round bottom 96-well plate, and cultured for 4 days. Anti-CD3 and anti-CD28 antibodies (1 µg/mL, eBioscience) were used for polyclonal activation. Polarizing conditions were as follows: Tc0 (cR10 media alone), Tc1 (1 ng/mL IL-2, 4 ng/mL IL-12, 1 µg/mL anti-IL-4), and Tc17 (50 ng/mL IL-6, 10 ng/mL TGF-β, 1 µg/mL anti-IFN-γ, 1 µg/mL anti-IL-4, 1 µg/mL anti-IL-2). All cytokines were from BioLegend. Anti-IL-4 antibody was from BioLegend (Cat. # 504108). After 4 days, cells were restimulated with

PMA (1 µM) and ionomycin (0.1 µM) in the presence of brefeldin (BioLegend) for 5 hours before intracellular FACS analysis of activation markers (IFN-γ, IL-17A). Data were acquired using a BD LSRII instrument.

ELISPOT assay

Detection of OVA-specific IFN-γ-secreting CD8⁺ T cells was performed using the ELISPOT assay, as described previously.³⁴ Ascites from ID8-OVA-bearing mice was harvested 8 weeks after tumor cells inoculation. CD8⁺ T cells were isolated with magnetic beads by using EasySep Mouse Naïve CD8⁺ T Cell Isolation Kit (Stemcell Technology, Cat. # 19853), according to the manufacturer's protocol. Cells were counted and seeded at 2×10⁵ cells/well in a Millipore plate (Cat. # S2EM004M99) and stimulated with/without OVA peptide (0.5 µg/mL). The control SIY peptide concentration was 5 µg/mL. The ELISPOT assay was performed 24 hours later according to the

manufacturer's instructions (eBioscience). Numbers and diameters of spots were measured in triplicate samples by an automatic ELISPOT counter.

T cell killing assay

CD8$^+$ T cells from ascites of TG2$^{+/+}$ (C57BL/6) and TG2$^{-/-}$ (TG2-KO) ID8-OVA tumor-bearing mice were enriched by negative selection using a CD8a$^+$ T Cell Isolation kit (Miltenyi Biotec, Cat. # 130-104-075) and LS magnetic columns. After selection, 10^5 CD8$^+$ T cells were sorted by FACS in duplicate for each genotype and co-cultured with ID8-OVA cells at 20:1 (effector:target) ratio to assess CD8$^+$ T cells killing capacity. Flow cytometry was used to determine apoptosis in the tumor cell fraction. For this, cells were washed with staining buffer (BioLegend, #420201) and subsequently were stained by using anti-CD45 Pacific Blue and anti-CD8 PerCP-Cy5.5 for 15 min at 4°C. After washing, cells were resuspended in 50 µL of Annexin binding buffer and double-stained with Annexin V-FITC/7-AAD (BioLegend, Cat. # 640922).

Flow cytometry and cell sorting

Ascites (40 µL) and single-cell suspensions of splenocytes ($3.5×10^6$ cells) were used for FACS analyses. Cells were incubated with 1 µg/mL antibody, washed twice with cold phosphate buffered saline (PBS), and fixed using BioLegend Fixation buffer. Nuclear Ki-67 and Foxp3 staining was performed according to the manufacturer's instructions (eBioscience). For OVA-specific dimer staining,[33] H-2kb:Ig Dimer X was loaded with 40 M excess of the OVA peptide and cells were stained according to the manufacturer's instruction (BD Bioscience) within the T cell differentiation panel. For pSTAT1/3/5 staining, cells were treated with IFN-γ (1 µg/mL), IL-6 (5 µg/mL), or TGF-β (1 µg/mL) for 15 min and then fixed in 1.5% para-formaldehyde for 10 min at RT.[34] Cells were centrifuged and resuspended in cold methanol for 10 min before storage at −80°C until staining.[35] Cells were washed twice with ice-cold PBS containing 1% bovine serum albumin (BSA). Anti-pSTAT antibodies were added for 30 min at RT together with those for surface markers in a final volume of 100 µL of ice-cold PBS and incubated at RT for 30 min. Cells were washed with staining buffer and analyzed by flow cytometry. Heatmaps were generated to show fold change of pSTATs in response to respective cytokine by using log10 ratio values of stimulated to unstimulated conditions. Median fluorescence intensity (MFI) of pSTATs was determined to acquire basal and stimulated expression levels before and after IL-6 stimulation, respectively, while the percentages were determined to evaluate the proportion of cells expressing the phosphoproteins. Uncompensated data were collected using either an LSRFortessa or an LSRII cytometer with FACSDiva software (both BD Biosciences). Compensation and analyses were performed using Cytobank (www.cytobank.org) or FlowJo V.10 software. UltraComp eBeads (ThermoFisher) were used for single color compensation. For some experiments, Zombie NIR Fixable Viability Dye was used (BioLegend) to stain PBS resuspended cells for live/dead discrimination. See supplemental material (SM) for additional details.

Colony formation assay

Post-seeding, ID8 cells were starved overnight and treated for 7 days with 20% or 50% pooled ascites supernatant or cultured in DMEM complete media. Media with 2×FBS was used to compensate for the ascites volume added to the wells. Day 7 pretreated cells were harvested and cultured for colony forming units assay at 150 cells per 60 mm dish for 10 days.

Apoptosis analysis

Ascites-treated ID8 cells for 5 days were FACS analyzed for apoptosis using Annexin V FITC/7-AAD double staining according to manufacturer's recommendations (BioLegend).

RNA sequencing (RNAseq)

Total RNA was extracted from EpCAM$^+$ epithelial cells sorted from ascites and from ascites-treated ID8 cells using the RNeasy Mini Kit (Qiagen, Cat. # 74104). See SM for details. Data are deposited in GEO (GSE139686).

Immunohistochemistry (IHC)

OC tissue microarray (TMA, #OVC1021) were obtained from Pantomics and stained for TG2 and CD8, as described in SM. TMAs were automatically scanned using the TissueFAXSiPlus imaging system (TissueGnostics, Vienna, Austria), and reconstituted virtual slides were subjected to quantitative image analysis (SM).

Image cytometry

From the 102 TMA cores, 15 specimens were excluded due to inadequate sample area or sample processing artifacts and 3 normal specimens were not included in the analysis. To quantify TG2, the scanned TMA was imported into the StrataQuest (V.5.0.1.336) image analysis software (TissueGnostics, Vienna, Austria) and processed with a customized analysis profile (APP) to differentiate epithelial from stromal tissue areas (online supplemental figure S2A) and to quantify the DAB signal (intensity and abundance) by using single-cell measurement masks and image cytometry scattergrams (online supplemental figure S2B) following a dedicated gating strategy (see SM). TG2 expression score was determined overall and within each tissue compartments using the formula: %TG2$^+$ cells*mean of single-cell mean pixel intensity of TG2. For estimating the numbers of CD8$^+$ T cells in the tumor or stromal compartments, tissue areas were inspected under 20X magnification. 'Cold' tissues were classified as 0, weakly infiltrated regions (<5–10 CD8$^+$ T cells) were scored as 1, and highly infiltrated specimens (>10 CD8$^+$ T cells) were scored as 2.

Statistical analyses

RNAseq data were analyzed using the Exact test which is based on quantile-adjusted conditional maximum

likelihood method in the edgeR package of R.[36] P values were adjusted for multiple hypotheses testing using false discovery rate (FDR) correction. The list of differentially expressed genes (FDR≤0.05) was uploaded into the Ingenuity Pathway Analysis (IPA, Ingenuity Systems) software to identify upstream regulators associated with the two conditions. Pathway analysis for the genes differentially expressed was performed with the web-based tool Enrichr (http://amp.pharm.mssm.edu/Enrichr/).[37] [38] The threshold for significance was set as a p value less than 0.05 and FDR at <30% (Fisher's exact test). The most significantly enriched pathways were displayed in R (V.4.0.3) (https://www.r-project.org/) using a horizontal bar chart. Significantly upregulated genes from Cholesterol Biosynthesis, Cholesterol Metabolism, and Interferon Signaling pathways were represented as red rose petals, the intensity of the red shade representing the magnitude of the fold change. The petals were generated with LaTeX (miKTex V.20.12) (https://miktex.org/). TGM2 RNA expression levels for different cell types were retrieved from the DICE (Database of Immune Cell Expression, Expression quantitative trait loci and Epigenomics) project (https://dice-database.org/). The Mann-Whitney-Wilcoxon test was applied to assess the relationship between TGM2 expression and different groups after testing for normality of the data with a Shapiro-Wilk test. Results are presented as box-and-whisker plots (boxes represent first and third quartiles, whiskers represent 1.5 times the IQR). Analyses were performed in R (V.3.5.1, http://www.r-project.org/) and statistical significance was set at p<0.05. Other experimental data from in vitro and in vivo experiments were analyzed by the Student's t-test. Kaplan-Meier analysis was applied to survival data. Correlation analyses were performed on the image cytometry TMA-derived data using the Pearson correlation coefficient. Analyses were performed in GraphPad Prism V.8 for Windows and V.9 for Mac (GraphPad software, San Diego, California, USA). Results are presented as mean±SEM, unless otherwise indicated. P values <0.05 were considered significant.

RESULTS

TG2 deficiency inhibited tumor progression in an OC syngeneic model

To determine whether TG2 expression in the host alters OC progression, the Roby syngeneic mouse model[39] was tested in TG2$^{-/-}$ mice. TG2 knockout was confirmed by PCR (online supplemental figure S1A) and western blotting (online supplemental figure S1B). ID8 cells were injected intraperitoneally in TG2 knockout (TG2$^{-/-}$) and wild-type (TG2$^{+/+}$) mice. Tumor burden was assessed at 6 weeks, when ascites became clinically detectable. Ascites volume (figure 1A, *p=0.0134) and number of cancer cells in ascites (figure 1B, *p=0.0187) were significantly decreased in TG2$^{-/-}$ versus TG2$^{+/+}$ mice, while miliary tumor dissemination on peritoneal surfaces was similar between TG2$^{-/-}$ and TG2$^{+/+}$ mice (figure 1C). ID8-bearing TG2$^{-/-}$ mice survived longer compared with controls

(*p=0.0209; median survival 47 days (n=12) vs 43 days (n=14), figure 1D).

TG2 deficiency promotes accumulation of effector CD8$^+$ T cells in ascites associated with OC

To determine whether the diminished tumor burden observed in TG2$^{-/-}$ mice was related to altered antitumor immune response, immune cell populations were characterized by flow cytometry at tumor site (in ascites) and in the spleens of tumor-bearing mice. FACS demonstrated a decrease in CD8$^+$ T cells in the spleens from TG2$^{-/-}$ mice compared with controls (figure 1E, *p=0.0144) and a corresponding increase in CD4$^+$ T cells proportion within the CD45$^+$ leukocytes fraction in ascites from TG2$^{-/-}$ mice versus TG2$^{+/+}$ controls (figure 1F, *p=0.0244). There were no significant differences in the percentage of CD4$^+$ T cells between TG2$^{+/+}$ and TG2$^{-/-}$ mice in spleens or ascites (figure 1E–F). A higher percentage of CD4$^+$ T regulatory cells (Treg) was detected in the spleens of TG2$^{-/-}$ mice (figure 1G, *p=0.0371), while a non-significant difference was observed in ascites (figure 1H). Activation of Tregs was observed in TG2$^{-/-}$ mice (figure 1G–H), with a significant increase in the percentage of GITR$^+$ Tregs (figure 1H, **p=0.0079). However, the CD8$^+$ T cells/Treg ratios in ascites and spleens (online supplemental figure S3A) were not different between TG2$^{+/+}$ and TG2$^{-/-}$ mice. In addition, higher percentages of PD-1$^+$ cells were detected among TG2$^{-/-}$ CD8$^+$ T cells versus controls, in both spleens and ascites (figure 1E–F, **p=0.0091 and *p=0.0272). The gating strategy for FACS is in online supplemental figure S3B. The results support that TG2 loss correlates with increased fraction of activated CD8$^+$ T cells in the peritoneal environment of OC-bearing mice. Cell counting revealed increased CD45$^+$ cell accumulation in ascites from TG2$^{-/-}$ mice, as well as increased number of all T cell subsets (figure 1I).

To determine whether TG2 deficiency alters the T cell compartments independent of cancer context, spleens of non-tumor-bearing mice were analyzed. Decreased CD8$^+$ and increased CD4$^+$ percentages were observed in TG2$^{-/-}$ versus control mice (online supplemental figure S3C, ***p=0.0007 and *p=0.0181). There were no measurable differences between Tregs and PD1 expressing CD8$^+$ T cells in the spleens of non-tumor-bearing TG2$^{-/-}$ versus control mice (online supplemental figure S3C). Gating strategy is shown in online supplemental figure S3D. These data support the presence of modest differences in the immune milieu associated with TG2 deficiency, as previously reported.[30]

TG2 deficiency enhances the cytotoxic function of CD8$^+$ T cells

To further determine the function of tumor-associated cytotoxic T cells, response to ex vivo stimulation was assessed. Ascites-derived TG2$^{-/-}$ CD8$^+$ and CD4$^+$ T cells demonstrated a significant threefold to fourfold increase in IFN-γ secreting cell fractions upon stimulation with ionomycin and PMA (figure 2A–B *p=0.0219 and **p=0.0044), as compared with controls. Interestingly,
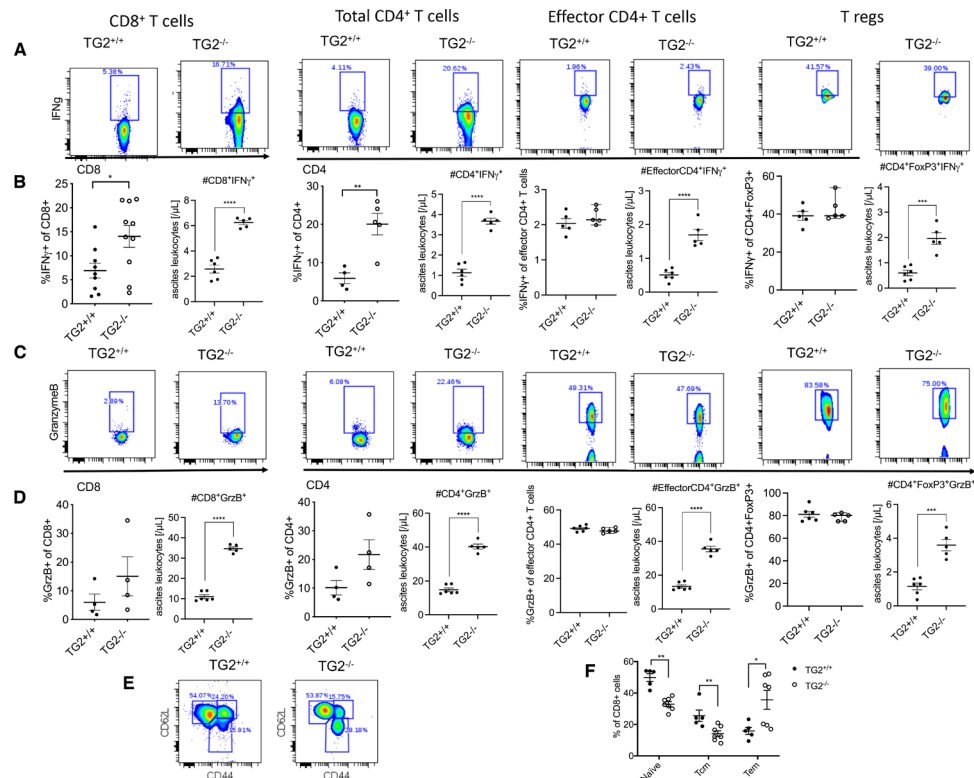
Figure 2 Tissue transglutaminase (TG2) deficiency enhances the effector function of CD8^{+} T cells isolated from ovarian cancer (OC)-associated ascites. (A, B) Representative flow cytometry density plots (A), and FACS quantification of percentages and counts (B) of IFN-γ secreting CD8^{+}, total CD4^{+} T cells, and subsets of effector CD4^{+} T cells and T regulatory cells (Tregs), on ex vivo restimulation (at least n=5 mice per group; *p<0.05, **p<0.005, ***p<0.001, ****p<0.0001). (C, D) Representative flow cytometry density plots (C), and FACS quantification of percentages and counts (D) of granzyme B secreting CD8^{+}, total CD4^{+} T cells, and subsets of effector CD4^{+} T cells and Tregs, on ex vivo restimulation (n=4 mice per group, one representative experiment; ***p<0.001, ****p<0.0001). (E, F) Representative flow cytometry density plots (E) and FACS analysis (F) of CD8^{+} T cell differentiation subsets (naïve, CD8^{+}CD62L^{hi}CD44^{low}; central memory, T_{cm}, CD8^{+}CD62L^{hi}CD44^{hi}; and effector/memory, T_{em}, CD8^{+}CD62L^{low}CD44^{hi}) among CD8^{+} T cells in ascites of TG2^{+/+} (n=5) and TG2^{−/−} (n=7) mice injected with ID8 cells. Data from two independent experiments are represented as means±SEM. *p<0.05; **p<0.005.

we found a greater accumulation of Tregs producing IFN-γ in ascites of tumor-bearing TG2^{-/-} mice compared with TG2^{+/+} mice, supporting a potential effect of TG2 on intrinsic IFN-γ-mediated Treg fragility to promote antitumor immunity[40] (figure 2A–B). Moreover, significantly increased absolute numbers, but not percentages, of granzyme B+ cells were observed in TG2^{-/-} lymphocytes (figure 2C–D). Spleen-derived T cells showed no significant difference in IFN-γ response between TG2^{-/-} and TG2^{+/+} cells (online supplemental figures S4A–B), but a significant increase in granzyme B secretion by spleen TG2^{-/-} CD8^{+} T cells stimulated ex vivo compared with TG2^{+/+} T cells was observed (online supplemental figure S4C,D, *p=0.0159), supporting increased effector function of TG2^{-/-} CD8^{+} T cells. However, no significant difference in T cell subsets restimulation between TG2 genotypes was noted in spleens of non-tumor-bearing mice (online supplemental figure S4E-L).

To identify whether TG2 deficiency affects T cell differentiation, we analyzed the distribution of CD8^{+} T cells between different subgroups in ascites from TG2^{-/-} versus TG2^{+/+} mice. These subsets are defined by specific markers that allow the quantification of CD8^{+} T cells residing in each differentiation stage from naïve-like (CD62L^{hi}CD44^{low}) to central memory (CD62L^{hi}CD44^{hi}) and effector/memory (CD62L^{low}CD44^{hi}) T cells. The effector/memory pool (T_{em}) was increased in ascites from TG2^{-/-} mice, while both the naïve-like (Naïve) and central memory (T_{cm}) CD8^{+} T cells pools were decreased compared with CD8^{+} T cells from TG2^{+/+} ascites (figure 2E–F, **p=0.0065, **p=0.0075, *p=0.0218). In spleen, there was an increase in naïve CD8^{+} T cells in TG2^{-/-} mice (*p=0.0208), with no significant difference observed between TG2^{-/-} and TG2^{+/+} mice for the other differentiated subsets (online supplemental figure S5A,B). Conversely, spleens of TG2^{-/-} mice showed decreased proportion of T_{cm} cells in tumor-free conditions (online supplemental figure S5C,D, *p=0.0248), suggesting a potential role of TG2 regulating CD8^{+} T cells differentiation. Ascites-sorted TG2^{-/-} CD8^{+} T cells had a higher capacity to recognize and kill ID8 tumor cells (more Annexin V^{+} apoptotic cells) in a co-culture experiment compared with TG2^{+/+} CD8^{+} T cells (online supplemental figure S5E). These results support that in the peritoneal TME, CD8^{+} T cells from TG2^{-/-} mice possess an enhanced effector T cell phenotype, differentiated towards the effector memory pool.

Decreased myeloid cells in the peritoneal TME of tumor-bearing TG2$^{-/-}$ mice

Myeloid cell subsets in spleens and ascites from TG2$^{-/-}$ and TG2$^{+/+}$ mice were also assessed. This population, including myeloid-derived suppressor cells (MDSCs) and tumor-associated macrophages (TAMs), negatively affects the antitumor immune response by inhibiting T cell cytotoxicity.[41] FACS demonstrated an overall tendency toward decreased CD11b$^+$ myeloid cell density within the TG2$^{-/-}$ ascites microenvironment (figure 3A–B, *p=0.0848). Within this population, decrease in granulocytic-type CD11b$^+$Gr1^{hi}Ly6C^{int} (G-MDSCs), monocytic-type CD11b$^+$Gr-1$^+$Ly6C^{hi} (M-MDSCs) MDSCs, and CD11b$^+$F4/80$^+$ TAMs was observed in the ascites from TG2$^{-/-}$ mice (figure 3A–B, *p=0.0301, *p=0.0353). The programmed death receptor ligand 1 (PD-L1) is expressed on the surface of antigen-presenting and myeloid cells in the TME and by engaging PD-1 on T cells, contributes to lymphocyte exhaustion.[42] There was a slight increasing trend in the percentages of PD-L1 expressing ascites-derived myeloid subsets in TG2$^{-/-}$ tumor-bearing mice (figure 3C–D, non-significant). In contrast to the peritoneal TME, myeloid cells were increased in the spleens of TG2$^{-/-}$ mice compared with controls (figure 4A–B, *p=0.0468). However, the MDSC subsets showed decreased percentages in TG2$^{-/-}$ spleens, more predominantly for G-MDSCs (figure 4B, *p=0.0061). PD-L1 expression was consistently decreased in the total splenic myeloid cell pool (figure 4C–D, **p=0.0053), as well as on all subsets (figure 4C–D, *p=0.0016, *p=0.0489) in TG2$^{-/-}$ mice compared with controls (figure 4D; online supplemental figure S6A, *p=0.0130). Gating strategies for MDSC subsets and TAMs are included in online supplemental figure S6B,C. In all, the results support that fewer immunosuppressive MDSCs and TAMs infiltrate the peritoneal TME in TG2$^{-/-}$ mice compared with controls.

## TG2 depletion enhanced antigen-specific antitumor T cell responses

To further characterize the effector phenotype of CD8$^+$ T cells in the TG2$^{-/-}$ background versus controls, antigen-specific T cell response was measured. For this, OVA-expressing ID8 cells were injected intraperitoneally in TG2$^{+/+}$ and TG2$^{-/-}$ mice, and OVA-specific CD8$^+$ T cell response was assessed by using Dimer-OVA staining and the ELISPOT assay. Increased percentages of CD8$^+$ T cells were detected in TG2$^{-/-}$ mice ascites (figure 5A, *p=0.0248). Further, the fraction of OVA-specific CD8$^+$ T cells was increased in ascites from TG2$^{-/-}$ mice as quantified by using Dimer-OVA staining (figure 5B; *p=0.0449). The ELISPOT assay measured IFN-γ secretion in magnetically separated ascites CD8$^+$ T cells recovered from ID8-OVA tumor-bearing mice (figure 5C–D). An increased response to OVA peptide stimulation was observed in TG2$^{-/-}$ T cells compared with controls (figure 5C and D, *p<0.0001). The data support that antigen-specific CD8$^+$ T cell response is more potent in TG2$^{-/-}$ mice versus controls ascites.

Antibody-mediated CD8$^+$ T cell depletion assessed the importance of CD8$^+$ T cells to the delayed tumor progression observed in TG2$^{-/-}$ mice. The experiment schema is included in online supplemental figure S7A, and CD8$^+$ T cell depletion was confirmed in ascites, whereas CD4$^+$ T cell numbers were not affected (online supplemental figure S7B). Depletion of CD8$^+$ T cells caused significant and faster ascites accumulation in TG2$^{-/-}$ compared with TG2$^{+/+}$ mice (figure 5E, *p=0.0352) with a trend toward increased number of cancer cells in ascites (figure 5F, p=0.0595), representing a reversal of the observed phenotype. The mice were sacrificed at an earlier point precluding detection of the expected difference in ascites accumulation in isotype-treated TG2$^{-/-}$ versus TG2$^{+/+}$ mice. The data support the concept that the delay in tumor progression in TG2$^{-/-}$ mice depends on enhanced CD8$^+$ T cell activity. The percentage of CD8$^+$ T cells resident in the spleens of both TG2$^{+/+}$ and TG2$^{-/-}$ mice subjected to CD8$^+$ T cell depletion decreased to ~20% for the TG2$^{+/+}$ and to ~40% for the TG2$^{-/-}$ mice, as compared with isotype-treated animals, with a slight accumulation of CD4$^+$ T cells (online supplemental figure S7C). Like non-treated (online supplemental figure S5A,B) and isotype IgG-treated mice (figure 5G-left panel), the persistent CD8$^+$ T cell fraction in the spleens of anti-CD8 treated TG2$^{-/-}$ mice included an enhanced T$_{naïve}$ (CD62L$^+$CD44$^-$) pool, compared with TG2$^{+/+}$ mice (mean % TG2$^{-/-}$ T$_{naïve}$ cells 67.95%>47.43% in TG2$^{+/+}$, **p=0.0066). CD8$^+$ T cells in spleens from TG2$^{-/-}$ mice retained the T$_{cm}$ fraction with no detectable alteration of their differentiation pattern (figure 5G–H, bottom panels), while TG2$^{+/+}$ splenocytes were almost depleted of this fraction upon anti-CD8 treatment (figure 5G–H, top panels, **p=0.0038, *p=0.0238). These results suggest a potential intrinsic role of TG2 in CD8$^+$ T cell differentiation.

Additionally, exploration of the publicly available transcriptomic Database of Immune Cell Expression,[43] comparing *TGM2* expression levels between immune cell subsets, revealed a 1.37-fold upregulation of *TG2 mRNA* in activated CD8$^+$ T cells as compared with inactive cells (figure 5I). *TGM2* transcript levels were also high in monocytes (online supplemental figure S7D) and in activated CD4$^+$ and Treg cells (online supplemental figure S7E), supporting a correlation between TG2 and immune responses.

TG2$^{-/-}$ CD8$^+$ T cells display altered STAT3 activation

To further understand the mechanism implicated in TG2-regulated CD8$^+$ T cell differentiation and activation in tumor-bearing hosts, STAT activation was measured. Ascites-derived T cells were stimulated ex vivo with cytokines commonly secreted in the OC TME (IFN-γ, TGF-β, and IL-6)[22 44] and which are representative for activating each STAT node. The engagement of JAK/STAT signaling, a pathway which plays an important role in regulation of T cell activation,[45] was assessed by phospho-flow cytometry. Steps of the gating strategy are presented in figure 6A. The heatmap in figure 6B
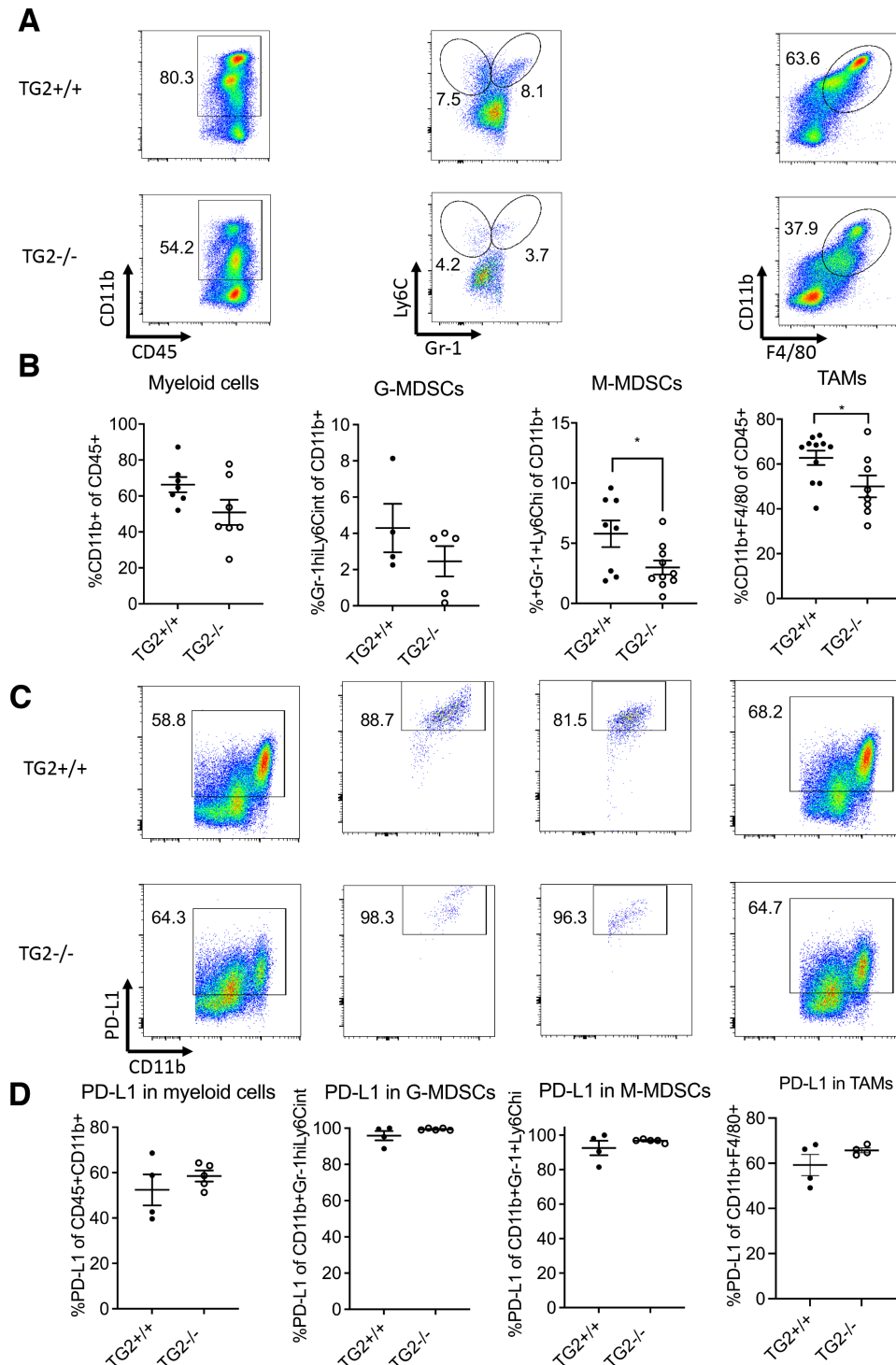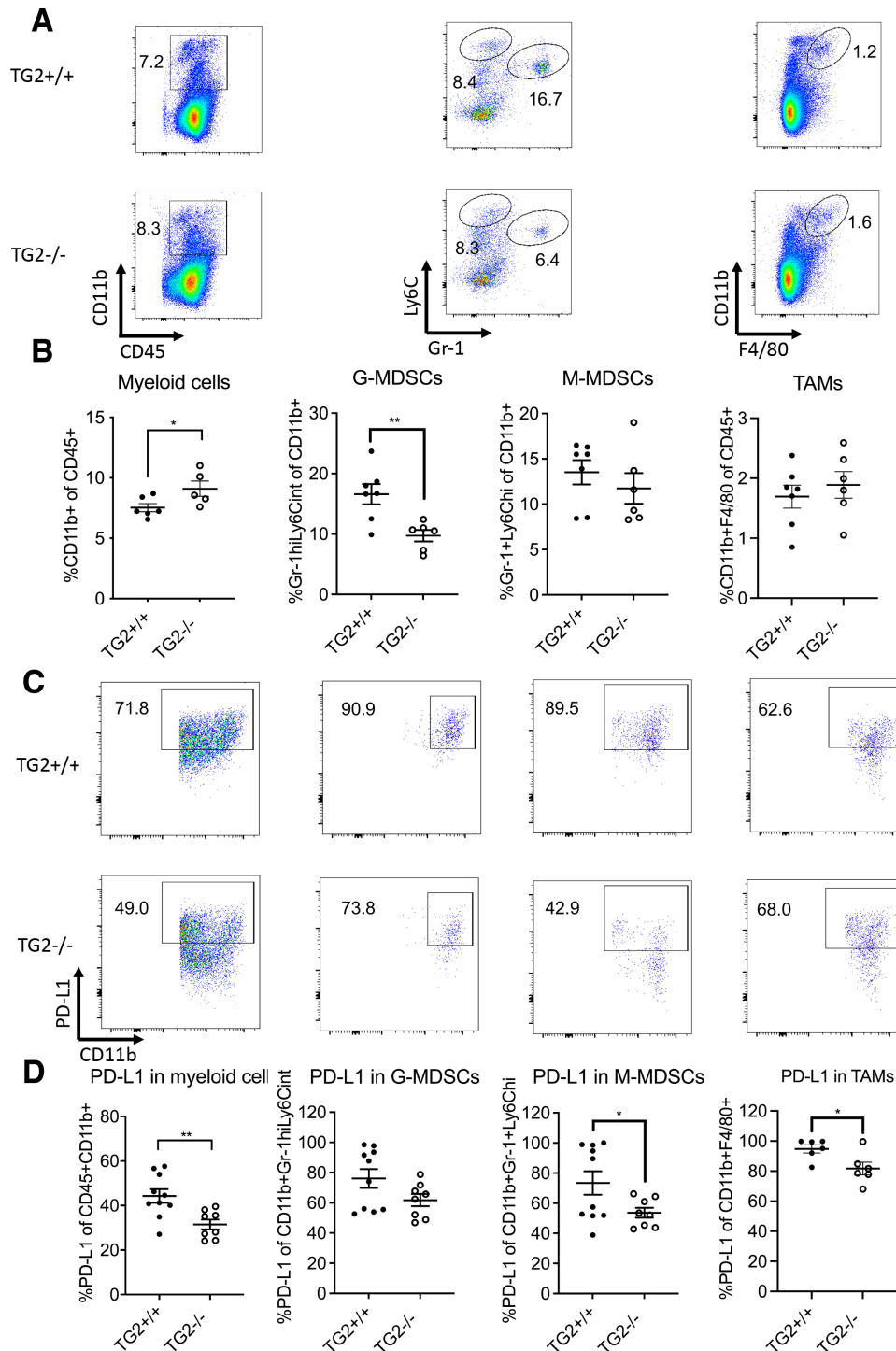
Figure 3 Myeloid cell populations in ascites of TG2$^{+/+}$ and TG2$^{-/-}$ tumor-bearing mice. (A, B) Flow cytometry analysis of myeloid cell populations in ascites: total myeloid cells (CD11b$^+$, n=7, two experiments), granulocytic myeloid-derived suppressor cells (G-MDSCs, CD11b$^+$Gr-1^{hi}Ly6c^{int}, n=5, one experiment), monocytic myeloid-derived suppressor cells (M-MDSCs, CD11b$^+$Gr-1$^+$LyBC^{hi}, n=9, two experiments), and tumor-associated macrophages (TAMs, CD11b^{hi}F4/80^{low}, n=11, three experiments). (C, D) FACS analysis of percentages of programmed death receptor ligand 1 (PD-L1) expressing cells within the total myeloid cell population and within the myeloid subpopulations G-MDSCs, M-MDSCs, and TAMs (n=4 for TG2$^{+/+}$ and n=5 for TG2$^{-/-}$, one representative experiment) in ascites. Data are presented as means±SEM. *p<0.05. TG2, tissue transglutaminase.

demonstrates differences in STAT-1, 3, and 5 phosphorylation in response to IFN-γ, TGF-β, and IL-6 in T cells from ascites collected from TG2$^{-/-}$ or TG2$^{+/+}$ mice.

STAT1 and STAT3 were activated more effectively in CD4$^+$ cells from TG2$^{+/+}$ compared with TG2$^{-/-}$ ascites in response to IFN-γ and TGF-β (figure 6B, upper panels).

Figure 4 Myeloid cell populations in spleens of TG2$^{+/+}$ and TG2$^{-/-}$ tumor-bearing mice. (A, B) Flow cytometry analysis of myeloid cell populations in the spleen: total myeloid cells (CD11b$^+$), granulocytic myeloid-derived suppressor cells (G-MDSCs, CD11b$^+$Gr-1^{hi}LyBC^{int}), monocytic myeloid-derived suppressor cells (M-MDSCs, CD11b$^+$Gr-1$^-$LyBC^{hi}), and tumor-associated macrophages (TAMs, CD11b^{hi}F4/80^{low}) (n=7, data from one representative experiment). (C, D) Fluorescence activated cell sorting (FACS) analysis quantified programmed death receptor ligand 1 (PD-L1) expressing cells in the total myeloid cell population (n=10, two experiments) and subpopulations: G-MDSCs (n=9, 2 experiments), M-MDSCs (n=10, two experiments), and TAMs (n=7, 1 experiment) from spleens. Data are presented as means ± SEM. *p<0.05 **p<0.005. TG2, tissue transglutaminase.

STAT3, but not STAT1, was phosphorylated more potently in response to IL-6 in CD4$^+$ cells from TG2$^{+/+}$ compared with TG2$^{-/-}$ ascites. Likewise, STAT3 phosphorylation was increased in response to all cytokines in CD8$^+$ cells from TG2$^{+/+}$ compared with TG2$^{-/-}$ ascites (figure 6B–C, online supplemental figure S8A), while activation of STAT1 appeared increased in CD8$^+$ cells from TG2$^{-/-}$ ascites (figure 6B, lower panels; figure 6C;
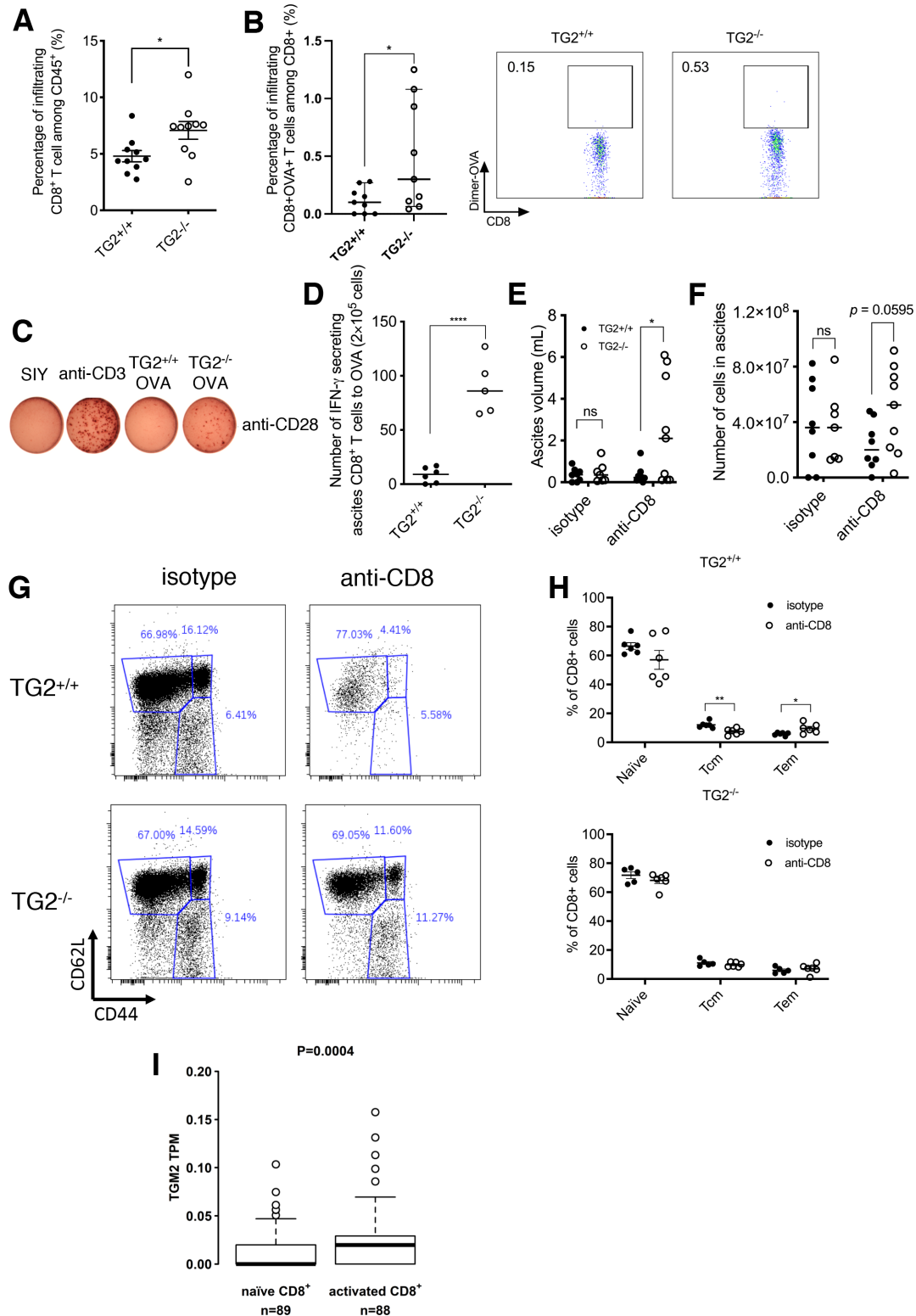
Figure 5 Antigen-specific T cell responses and in vitro T cell differentiation of TG2$^{+/+}$ and TG2$^{-/-}$ CD8$^+$ T cells. (A). Flow cytometry quantification of total CD8$^+$ T cells infiltrated into ascites of TG2$^{+/+}$ and TG2$^{-/-}$ mice (n=10, *p<0.05). (B) OVA-specific CD8$^+$ T cells infiltrated into ascites, and representative flow cytometry dot plots depicting OVA-specific CD8$^+$ T cells fractions detected by dimer-OVA staining in ascites of TG2$^{+/+}$ and TG2$^{-/-}$ mice (n=10, *p<0.05). (C, D) ELISPOT assay quantifies numbers of IFN-γ-secreting CD8$^+$ T cells in the ascites of TG2$^{+/+}$ (n=6) and TG2$^{-/-}$ (n=5) mice responding to OVA peptide stimulation. ****p<0.0001. (E, F) Tumor burden assessment (as in figure 1A,B) in mice on depletion of CD8$^+$ T cells includes assessment of ascites volumes (n=9, *p<0.05) and numbers of cells (n=9, p=0.0595). Data represent three independent experiments. (G, H) Representative dot plots and summary of CD8$^+$ T cell differentiation subsets in TG2$^{-/-}$ versus TG2$^{+/+}$ spleens at the end of CD8$^+$ T cell depletion treatment. (I) Expression levels of *TGM2* in activated and naïve CD8$^+$ T cells extracted from the DICE database. P values were obtained by using the Mann-Whitney test. TG2, tissue transglutaminase.
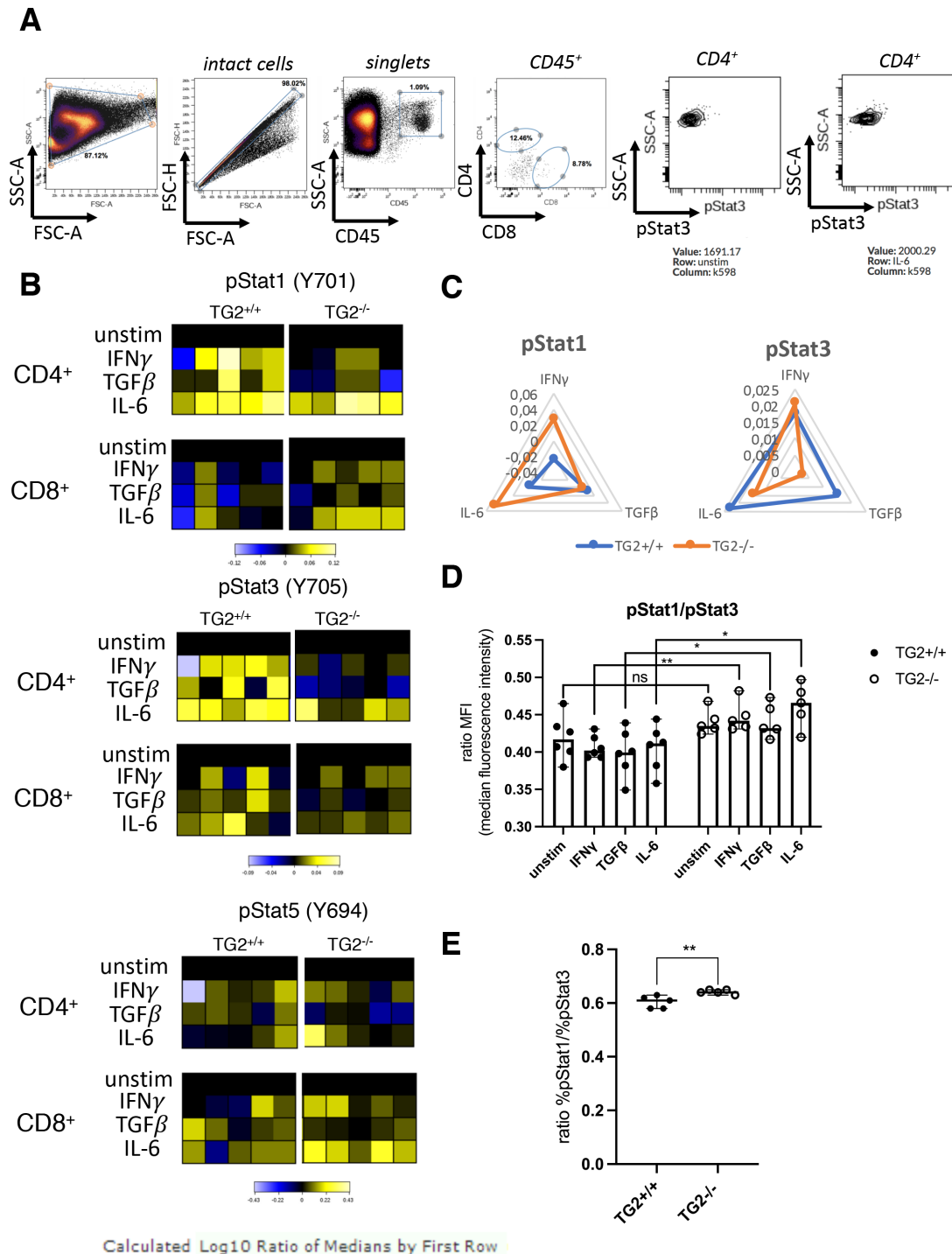
Figure 6 STAT activation in TG2^{+/+} and TG2^{-/-} T cells. (A) Ascites cells from tumor-bearing mice were either left unstimulated or stimulated with cytokines. Density plots show the gating strategy for measuring phosphorylated STAT in T cells isolated from ascites. Example of pSTAT3 signal detected in CD4^{+} T cells before (median fluorescence intensity (MFI)=1691.17) and after (MFI=2000.29) IL-6 stimulation by using Cytobank generated contour plots. (B) Analysis of cytokine-induced phosphorylation of STAT proteins. MFI (log10 fold-change) of pStat1, pStat3, and pStat5 in ascites-derived CD4^{+} and CD8^{+} T cells from tumor-bearing TG2^{+/+} or TG2^{-/-} mice (n=5 per condition, shown are data from one representative experiment), stimulated for 15 min with IFN-γ (1 µg/mL), transforming growth factor (TGF-β) 1 µg/mL), or IL-6 (5 µg/mL). Protein phosphorylation is represented as a heatmap using the Cytobank platform. Each square represents the response of a specific STAT protein to the respective cytokine in a distinct cell type. The scale is specific to each pSTAT and consistent across cell types and represented beneath as blue to yellow color code (log10 ratio of medians). (C) Radar plots of pStat1 and pStat3 levels in B (median of log10 ratios) in CD8^{+} T cells from TG2^{+/+} and TG2^{-/-} mice on IFN-γ, TGF-β and IL-6 cytokine stimulation. Blue indicates TG2^{+/+}, while orange represents TG2^{-/-}. (D) Quantification of pStat1/pStat3 MFI ratio before and after cytokine stimulation in CD8^{+} T cells isolated from ascites of TG2^{-/-} and TG2^{+/+} mice (*p<0.05, **p<0.01). (D) Quantification of pStat1/pStat3 percentages ratio in unstimulated CD8^{+} T cells isolated from ascites of TG2^{-/-} and TG2^{+/+} mice (**p<0.01). TG2, tissue transglutaminase.

online supplemental figure S8B, *p=0.049, *p=0.011). A significant increase in the ratio of pSTAT1/pSTAT3 levels (figure 6D, **p=0.004, *p=0.031, *p=0.011) in response to IFN-γ, IL-6, and TGF-β was detected in CD8$^+$ cells from TG2$^{-/-}$ compared with TG2$^{+/+}$ ascites. Of note is that under unstimulated conditions, the ratio of %pSTAT1/%pSTAT3 within CD8$^+$ T cells was already increased (figure 6E, *p=0.0085). There were no measurable differences in STAT5 activation in either CD4$^+$ and CD8$^+$ T cells from TG2$^{-/-}$ versus TG2$^{+/+}$ in response to the three cytokines (figure 6B, online supplemental figure S8C). These results suggest the potential involvement of TG2 in differential activation of STAT1 versus STAT3 to fine tune the effector function of T cells (figure 6C–E).

We next investigated the possibility that TG2 could affect the intrinsic capacity of CD8$^+$ T lymphocytes to polarize and differentiate to effector cells on activation signals. First, we quantified under Tc0 conditions the expression of two key reprogramming transcription factors T-bet[46] and Gata-3.[47] There was an increasing trend in expression of both factors in TG2$^{-/-}$ versus TG2$^{+/+}$ CD8$^+$ T cells isolated from the spleens of tumor-free mice (figure 7A–B). When assessing differentiation toward Tc1, an increased percentage of IFN-γ secreting Tc0 and Tc1 polarized CD8$^+$ T cells was observed in TG2$^{-/-}$ compared with TG2$^{+/+}$ mice (figure 7C and D, ****p<0.0001). Similarly, increased percentages of IL-17A secreting Tc0 and Tc17 polarized CD8$^+$ T cells were detected in TG2$^{-/-}$ versus TG2$^{+/+}$ mice (figure 7C and E, *p<0.05, ***p<0.001).

Splenic CD8$^+$ T cells isolated from tumor-free TG2$^{+/+}$ and TG2$^{-/-}$ mice were cultured in Tc0 conditions for 4 days prior to IL-6 stimulation. Decreased STAT3 phosphorylation was observed in TG2$^{-/-}$ versus TG2$^{+/+}$ cytotoxic T cells (figure 7F). To determine whether the enzymatic activity of TG2 plays a role in regulating STAT3 activation in CD8$^+$ T cells, two specific TG2 transamidase inhibitors (ERW1041E and NC9)[48 49] were used during Tc0 polarization of TG2$^{+/+}$ CD8$^+$ T cells. Both inhibitors decreased STAT3 phosphorylation (figure 7G), consistent with the phenotype observed in TG2$^{-/-}$ models (figure 6B–E), suggesting that the enzymatic function of TG2 may contribute to the observed phenotype. Together, the results support an inhibitory role of TG2 in the differentiation of cytotoxic T cells mediated likely through STAT3.

Effects of host TG2 on tumor cells in the peritoneal environment

We next evaluated whether TG2 expression in the tumor stroma affected CD8$^+$ T cell intratumoral infiltration. We used a cohort of 84 human OC specimens arrayed on a TMA and assessed TG2 expression by IHC in cancer cells and in the stroma. Intratumoral CD8$^+$ T cell infiltration was graded as 0, 1, and 2, based on numbers of detectable CD8$^+$ T cells (figure 8A). Stromal TG2 expression correlated negatively with intratumor CD8$^+$ T cell infiltration in human OC specimens (r=−0.2252, *p=0.0360,

figure 8A–B), like observations in the immunocompetent animal model.

To determine the global effects of host TG2 depletion on tumor cells in the peritoneal environment, sorted EpCAM$^+$ cells from TG2$^{-/-}$ and TG2$^{+/+}$ ascites (online supplemental figure S9A) were analyzed by RNA sequencing. The analysis revealed 921 transcripts differentially expressed, p<0.05, fold-change >2 (online supplemental tables 2,3) and hierarchical clustering showed distinct transcriptomic profiles of tumor cells harvested from TG2$^{-/-}$ and TG2$^{+/+}$ mice (figure 8C). Upregulation of genes related to antigen presentation and immune response was observed in EpCAM$^+$ cells separated from TG2$^{-/-}$ compared with cells isolated from TG2$^{+/+}$ ascites (online supplemental table S2). Among them, interferon inducible *GTPase 1 (Iigp1), Immunity-related GTPase family M member 2 (Irgm2), Interferon gamma induced GTAse (Igtp), interferon induced protein 44 (Ifi44)*, and *STAT1* were among the genes significantly (FDR<0.01) upregulated (>3-fold) in cancer cells from TG2$^{-/-}$ ascites (online supplemental table S2), reflecting a gene signature responsive to IFN-γ secreted in the peritoneal TME of TG2$^{-/-}$ mice. Enrichr analysis of differentially expressed genes revealed enrichment in *Metabolism of Lipids and Lipoproteins, Interferon Signaling, Cholesterol Biosynthesis Pathways, Antigen Processing and Presentation Pathways* (figure 7D). Conversely, pathways involved in *Glycolysis and Gluconeogenesis, HIF1-α Transcription Factor Network,* and *Tumor Infiltrating Macrophages in Cancer Progression and Immune Escape* were downregulated (figure 8E). Among the top upstream regulators identified by using IPA, IFN-γ was activated, whereas lipopolisaccharide (LPS), TP53, and TGF-β1 were inhibited in epithelial cells from TG2$^{-/-}$ mice (online supplemental figure S9B). Transcripts involved in *Interferon Signaling* (figure 8F), *Cholesterol Biosynthesis,* and *Cholesterol Metabolism* (online supplemental figure S9B) were significantly upregulated in the cancer cells from ascites from TG2$^{-/-}$ compared with TG2$^{+/+}$ mice. Genes related to cell homing, adhesion, and invasion were downregulated in EpCAM$^+$ cells from TG2$^{-/-}$ versus TG2$^{+/+}$ ascites (online supplemental table S3). The data suggest that cancer cells in the TG2$^{-/-}$ peritoneal environment are likely more visible and more vulnerable to immune attack, while simultaneously being less invasive.

To further test the effects of ascites on tumor cells, colony forming, cell cycle, and apoptosis assays were performed after ex vivo treatment of ID8 cells with ascites from tumor-bearing TG2$^{-/-}$ and TG2$^{+/+}$ mice. Ascites from TG2$^{-/-}$ mice inhibited colony formation more potently than ascites from TG2$^{+/+}$ control mice (figure 8G). On treatment with TG2$^{-/-}$ ascites, a modest decrease in the cell population transiting from S to G2/M phase was observed (online supplemental figure S9C) along with a significant increased apoptosis of ID8 cells (figure 8H and online supplemental figure S9D). Collectively, these data support that the proliferation and survival of cancer cells are negatively affected by TG2$^{-/-}$ ascites.
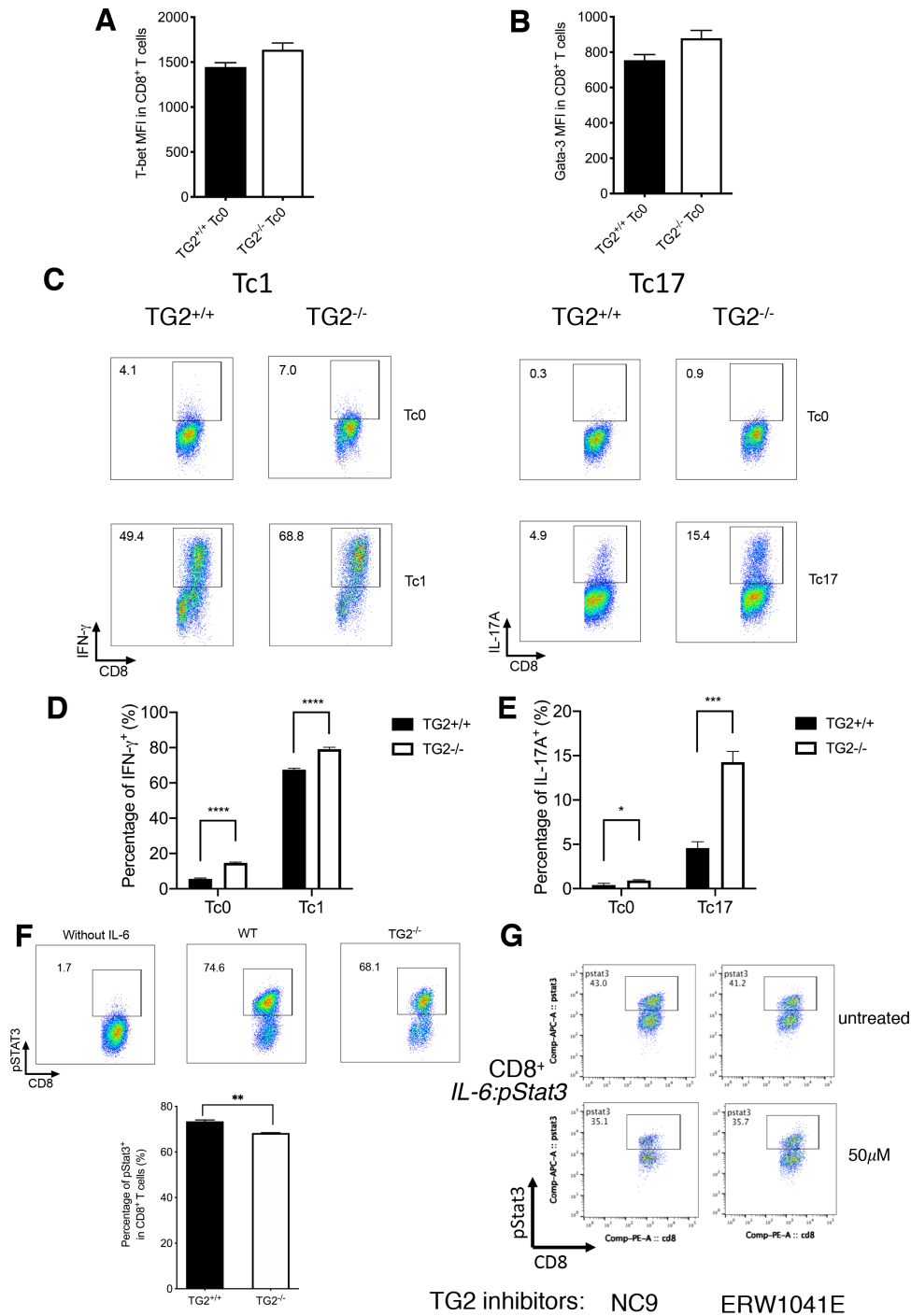
Figure 7 Intrinsic CD8^{+} T cell modifications produced by tissue transglutaminase (TG2) targeting. (A, B) Percentage of T-bet (n=4) and Gata-3 (n=3) expressing CD8^{+} T cells determined by flow cytometry in Tc0 polarized cells from TG2^{+/+} and TG2^{-/-} mice spleens. One representative experiment is represented. (C) Representative dot plots of IFN-γ and IL-17A secreting CD8^{+} T cells determined by flow cytometry in Tc1 versus Tc0 (left) and Tc17 versus Tc0 (right) polarization conditions, respectively, from TG2^{+/+} and TG2^{-/-} mice. (D, E) Percentage of IFN-γ and IL-17A secreting CD8^{+} T cells determined by flow cytometry in Tc1 versus Tc0 (H) and Tc17 versus Tc0 (I) polarized fractions, respectively, from TG2^{+/+} and TG2^{-/-} mice (n=3). Data represent one experiment out of two performed. (F) STAT3 activation status in CD8^{+} T cells isolated from naïve TG2^{+/+} and TG2^{-/-} mice activated using anti-CD3 and anti-CD28 antibodies (Tc0), and stimulated with 10 ng/mL IL-6 before analysis. (G) Effects of TG2 inhibitors (NC9 and ERW1041E) on STAT3 activation in CD8^{+} T cells isolated from naïve TG2^{+/+} mice and treated as in E. *p<0.05; **p<0.01; ***p<0.001; ****p<0.0001.

The morphology of ID8 cells treated with TG2^{-/-} ascites changed toward a mesenchymal appearance, with accumulation of intracellular *vacuolae*, indicating cytotoxicity (online supplemental figure S10A). RNA sequencing also compared the transcriptomic profiles of ID8 cells treated with TG2^{-/-} versus TG2^{+/+} ascites. Distinct transcriptomic
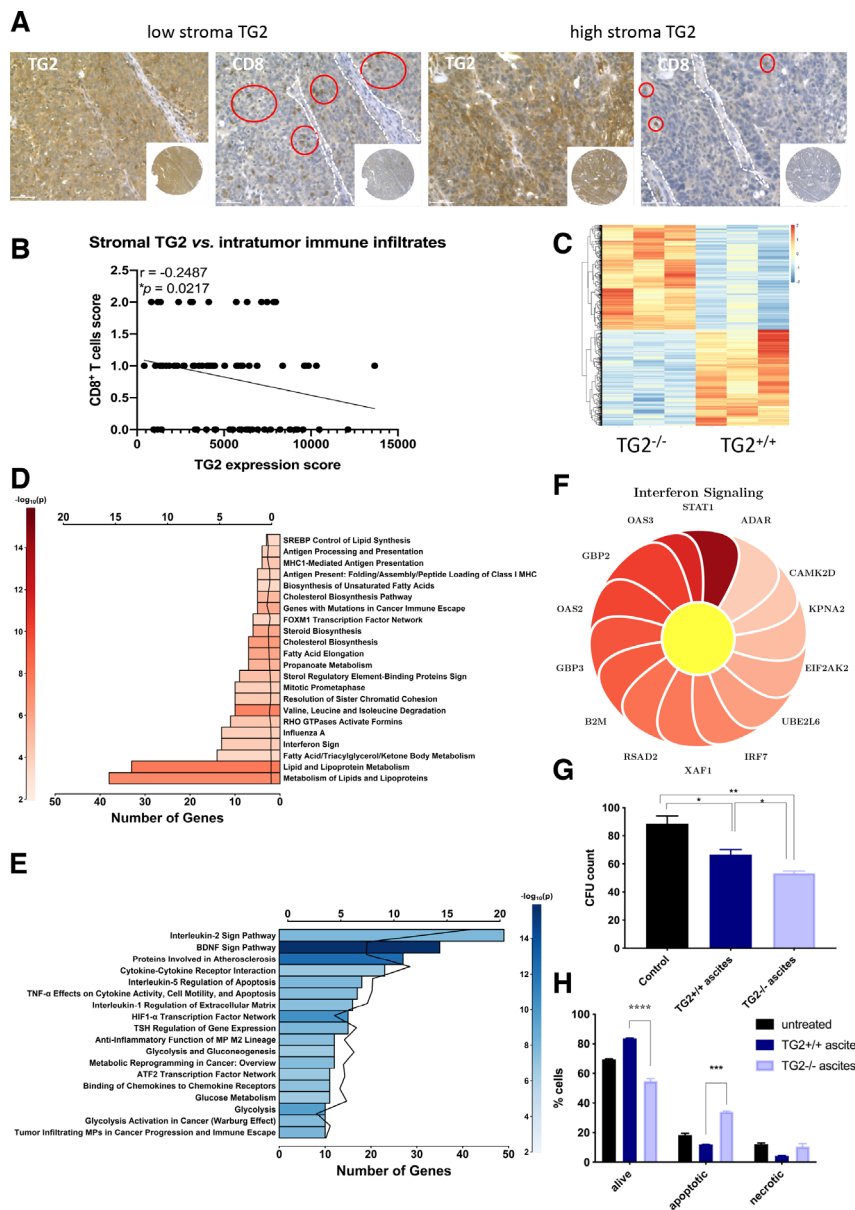
Figure 8 Effects of tissue transglutaminase (TG2) expressed in the tumor microenvironment (TME) on tumor cells. (A) Representative fields showing IHC staining for TG2 and CD8 in human OC specimens on a tissue microarray (TMA) (n=84). Representative paired specimens show TG2 and CD8 expression in tumors with low (left) and high (right) stromal TG2 expression. Stroma is delimited by white dashed contours and CD8^{+} T cells are indicated by red circles. Insets depict the whole TMA spots. (B) Indirect correlation between stromal TG2 expression level and level of intratumoral CD8^{+} T cell infiltration (*p=0.0217, r=−0.2487). (C) Unsupervised hierarchical clustering shows gene expression profiles measured by RNAseq in sorted EpCAM^{+} cells from ascites of TG2^{−/−} and TG2^{+/+} mice inoculated with ID8 cells (n=3 specimens per group). (D, E) Enriched pathways upregulated (F) or downregulated (E) in sorted EpCAM^{+} cells from ascites of TG2^{−/−} versus TG2^{+/+} mice. The bar chart illustrates the number of differentiated genes on each pathway, the ratio of the number of differentiated genes to the total number of genes known on the pathway, and the p value of the Fisher test. (F) Representation of the fold change (FCH) for the genes associated with interferon, with different shades of red as they were upregulated, the intensity of the color representing the magnitude of fold change; petals are arranged according to the fold change. (G) Colony formation assay for ID8 cells cultured in media containing ascites pooled fromTG2^{+/+} or TG2^{−/−} mice (n=8). (H) Flow cytometry using Annexin V/7AAD double labeling quantifies apoptosis in ID8 cells treated with ascites pooled from TG2^{+/+} or TG2^{−/−} mice. Data are represented as means±SEM (*p<0.05; **p<0.05; ***p<0.001; ****p<0.0001).

profiles were evident in ID8 cells treated ex vivo with TG2^{−/−} versus TG2^{+/+} ascites (online supplemental figure S10B) with the top enriched pathways in TG2^{−/−} versus TG2^{+/+} ascites-treated cells being *Cholesterol Biosynthesis* and *Immune Response* (online supplemental figure S10C,

online supplemental tables S4,5) similar to the transcriptomic profiles of cancer cells isolated from ascites. While we suspected that secreted factors in ascites were responsible for the observed changes, no significant differences in IL-6 and IFN-γ concentrations were detected in ascites

collected from TG2^{-/-} versus TG2^{+/+} tumor-bearing mice (online supplemental figure S10D). In all, the data support that when TG2 is absent in the peritoneal TME, tumor cells are less likely to survive and undergo apoptosis, due to enhanced immune surveillance.

DISCUSSION

We describe a previously unappreciated function of TG2 as an attenuator of antitumor immunity. In parallel to significant decrease in tumor burden detected in OC syngeneic models, increased numbers of active cytotoxic lymphocytes differentiated toward an effector phenotype were observed in malignant ascites collected from TG2^{-/-} mice compared with controls. TG2 knockout, or its enzymatic inhibition in CD8^{+} T cells, led to reduced cytokine-induced STAT3 phosphorylation, a known inhibitory T cell signal. In all, our studies reveal a new mechanism by which TG2 modulates T cell immunity and tumor progression in OC models. Our findings have several implications.

First, to our knowledge, the effects of TG2 on the antitumor immune response have not been previously assessed. We had identified TG2 as an adhesion protein overexpressed in cancer cells and at their interface with the TME and demonstrated its metastasis promoting role in this context.[4 5] The role of TG2 modulating the behavior of cancer cells was also reported in other solid tumors, with high levels of the enzyme being generally correlated with unfavorable prognosis.[11 20 44 50 51] Using genetic knockdown models and pharmacological inhibitors, we and others have shown that TG2 inhibition blocks cancer cell spheroid formation and tumor progression.[5 23 52] However, contradictory results were reported when TG2 was knocked out in the host. In a subcutaneous syngeneic model of melanoma, accelerated tumor progression was observed in TG2^{-/-} mice[53] through a mechanism dependent on lack of stroma crosslinking and stimulation of angiogenesis induced by deficiency of the active enzyme. In another report, accelerated melanoma progression in TG2^{-/-} mice was attributed to the lost interaction between TG2 and the G-protein coupled receptor GPR56, with tumor suppressor functions.[54]

By conducting immune profiling of cells recovered from the ascites of TG2^{+/+} and TG2^{-/-} tumor-bearing mice, here we describe the impact of TG2 on the peritoneal immune cell populations and their functions in OC. Our results demonstrating increased accumulation and enhanced effector function of CD8^{+} and CD4^{+} cells in TG2^{-/-} mice-bearing ovarian tumors are consistent with the known phenotype of these mice, which display increased auto-immunity with age[25] and clear infections, such as *M. tuberculosis*, more effectively.[26] In those contexts, however, the role of TG2 was linked to the deficient function of macrophages clearing apoptotic bodies or mycobacteria, with limited evaluation of the T cell function. TG2 was shown recently to facilitate the interaction between dendritic cells and T cells leading to more potent responses to antigen stimulation.[27] Interestingly, here we detected an increase in the T effector/memory (T_em) pool in the ascites recovered from TG2^{-/-} mice, as well as a propensity of the CD8^{+} T cell fraction from the spleens of TG2^{-/-} naïve tumor-free mice to differentiate toward a Tc1 fate. It had been established that in the context of antitumor immune response, T_em cells exhibit rapid effector function, readily differentiating into IFN-γ secreting T effector cells (T_eff) with enhanced cytotoxicity.[55] It is possible that complete deficiency of the enzyme in the knockout animal creates a more vulnerable state, which is compensated through other mechanisms, such as enhanced immune responses. Additionally, we noted an increase in TG2 expression level in human activated CD8^{+} T cells compared with inactive cells, based on bioinformatic analyses, corroborating our findings from animal experiments. Lastly, IHC of human OC specimens showed a negative correlation between TG2 expression in the stroma of ovarian tumors and intratumoral CD8^{+} T cell infiltration, further supporting the proposed concept.

Second, we found that absence of TG2 attenuates STAT3 phosphorylation in CD8^{+} and CD4^{+} T cells in response to IL-6, IFN-γ, and TGF-β, cytokines abundantly secreted in the peritoneal microenvironment.[22 56] To analyze JAK-STAT intracellular signaling, we used phospho-flow, a highly sensitive technique,[57] and observed that STAT3, but not STAT1 or STAT5, was less responsive to cytokine stimulation in T cells collected from the ascites of TG2^{-/-} mice. The distinction between immune responses that suppress and promote cancer is regulated by the STAT family members. In particular, STAT1 activation leads to enhanced TH1-type responses and CD8^{+} T cell-mediated cytolytic activity, which is often antagonized by STAT3.[58–60] STAT3 has emerged as a critical regulator for CD8^{+} T-cell cytotoxic capacities and their tumor infiltration.[61 62] STAT3 depletion in CD8^{+} T cells was shown to alter the cross-talk between effector T cells and myeloid cells through IFNγ/CXCR3/CXCL10 axis, resulting in efficient accumulation of CD8^{+} T cells in the tumor milieu.[63] Activation of STAT3 in antigen presenting cells caused impaired antigen-specific T cell responses, while its depletion decreased T cell anergy.[64] In the TME, STAT3 activation was shown to alter the balance between IL-23 secretion from TAMs and IL1-2 production from dendritic cells, leading to decreased antitumor immunity.[65] However, STAT3 was also shown to play an important role preserving the T memory cell function by sustaining the expression of 'pro-memory' transcription factors.[66] STAT3 ablation in CD8^{+} T cells prior to adoptive transfer allowed efficient in vivo tumor infiltration and robust proliferation, resulting in increased tumor antigen-specific T-cell activity and tumor growth inhibition in melanoma and renal cell carcinoma.[61] The effects of TG2 on STAT3 signaling have been previously unexplored. A single report noted that TG2 affected IL-6/Stat3 signaling in mantle cell lymphoma cells, decreasing autophagy.[67] Our experiments using TG2 inhibitors which inactivated STAT3 in CD8^{+} T cells suggest that the

enzymatic function of the protein may be important for regulating this pathway. These data suggest that therapeutic interventions targeting TG2 have the potential to tip the balance of STAT1/STAT3 to augment antitumor CD8$^+$ T cell immunity.

Third, we observed significant changes in the transcriptomic profiles of cancer cells generating tumors in TG2$^{-/-}$ mice and of tumor cells treated ex vivo with TG2$^{-/-}$ ascites, including significant increase in IFN-γ response genes and alterations of *Cholesterol Synthesis* and *Antigen Presentation* pathways. Upregulation of IFN responsive genes (*Iigp1, Irgm2, Igtp, Ifi44, STAT1,* and others) reflects that cancer cells in the peritoneal milieu of TG2$^{-/-}$ mice respond to the IFN-γ attack initiated by activated CD8$^+$ T cells. IFN-γ was the top upstream regulator in the gene network differentially expressed in cancer cells grown in TG2$^{-/-}$ versus control mice. Further, *Cholesterol Synthesis* was found to a consistently upregulated pathway in cancer cells recovered from TG2$^{-/-}$ ascites. Recent data suggest that cholesterol derivatives in tumor cells could regulate immune recognition and the activity of immune cells in the TME.[68] Cholesterol is a key element of lipid rafts, which contain among other receptors, major histocompatibility complex molecules and toll like receptors, perhaps facilitating immune recognition of cancer cells. A proinflammatory TME like the conditions observed in the TG2$^{-/-}$ peritoneal milieu was shown to upregulate cholesterol synthesis in liver cancer models.[69] It is also possible that under the attack of cytotoxic T cells in the TG2$^{-/-}$ environment, OC cells upregulate lipid metabolic pathways as an escape survival mechanism.

Lastly, we detected fewer MDSCs and TAMs in the peritoneal microenvironment of TG2$^{-/-}$ mice compared with controls, suggesting that the milieu of tumors developing in these animals is less immunosuppressive. TG2 was shown to be enriched in M2 monocytes,[70] as we also found here through bioinformatic exploration of a public database. These findings may explain the decrease in number of cells of monocytic lineage being attracted to the TME in TG2$^{-/-}$ animals. Interestingly, presence of PD-L1–expressing dendritic cells and macrophages is recognized as a factor contributing to tumor immune tolerance and is emerging as a potential predictor of response to immune checkpoint inhibitors in OC and other models.[71] The observations that PD-L1 expression on myeloid cells is reduced in a TG2 null context could fuel speculations that TG2 blockade may be investigated as a potential modality of blocking this immune inhibitory pathway.

In summary, here we describe a new role of TG2 regulating the host antitumor response by altering the effector function of CD8$^+$ T cells and reducing the immunosuppressive myeloid cell populations in the peritoneal environment of tumor-bearing mice. Mechanistically, we show that absence of TG2 caused dampened STAT3 signaling in response to local cytokines in CD8$^+$ and CD4$^+$ T cells. We propose TG2 as a novel molecular target for manipulating immune activation/tolerance in the context of cancer. Our studies have implications for understanding autoimmunity, antitumor immunity, and perhaps, for refining cancer immunotherapy.

Author affiliations
[1]Department of Obstetrics and Gynecology, Northwestern University Feinberg School of Medicine, Chicago, Illinois, USA
[2]Department of Molecular Cell Biology, Institute of Biochemistry of the Romanian Academy, Bucharest, Romania
[3]Department of Medicine; Hematology/Oncology Division, Northwestern University Feinberg School of Medicine, Chicago, Illinois, USA
[4]Department of Experimental Therapeutics, Center for RNA Interference and Non-Coding RNA, The University of Texas MD Anderson Cancer Center, Houston, Texas, USA
[5]Robert H. Lurie Comprehensive Cancer Center, Northwestern University Feinberg School of Medicine, Chicago, Illinois, USA
[6]Jesse Brown Veterans Affairs Medical Center, Chicago, IL, USA

ORCID iDs
Livia Elena Sima http://orcid.org/0000-0002-3404-4162
Guangyuan Zhao http://orcid.org/0000-0002-1095-8875

REFERENCES
1 Huang X, Lin T, Gu J, *et al*. Combined TRAIL and Bax gene therapy prolonged survival in mice with ovarian cancer xenograft. *Gene Ther* 2002;9:1379–86.
2 Stephens P, Grenard P, Aeschlimann P, *et al*. Crosslinking and G-protein functions of transglutaminase 2 contribute differentially to fibroblast wound healing responses. *J Cell Sci* 2004;117:3389–403.

3 Fesus L, Piacentini M. Transglutaminase 2: an enigmatic enzyme with diverse functions. *Trends Biochem Sci* 2002;27:534–9.

4 Satpathy M, Cao L, Pincheira R, *et al*. Enhanced peritoneal ovarian tumor dissemination by tissue transglutaminase. *Cancer Res* 2007;67:7194–202.

5 Shao M, Cao L, Shen C, *et al*. Epithelial-to-mesenchymal transition and ovarian tumor progression induced by tissue transglutaminase. *Cancer Res* 2009;69:9192–201.

6 Iacobuzio-Donahue CA, Ashfaq R, Maitra A, *et al*. Highly expressed genes in pancreatic ductal adenocarcinomas: a comprehensive characterization and comparison of the transcription profiles obtained from three major technologies. *Cancer Res* 2003;63:8614–22.

7 Derynck R, Zhang YE. Smad-dependent and Smad-independent pathways in TGF-beta family signalling. *Nature* 2003;425:577–84.

8 Martinet N, Bonnard L, Regnault V, *et al*. In vivo transglutaminase type 1 expression in normal lung, preinvasive bronchial lesions, and lung cancer. *Am J Respir Cell Mol Biol* 2003;28:428–35.

9 Grigoriev MY, Suspitsin EN, Togo AV, *et al*. Tissue transglutaminase expression in breast carcinomas. *J Exp Clin Cancer Res* 2001;20:265–8.

10 Verma A, Wang H, Manavathi B, *et al*. Increased expression of tissue transglutaminase in pancreatic ductal adenocarcinoma and its implications in drug resistance and metastasis. *Cancer Res* 2006;66:10525–33.

11 Hwang JY, Mangala LS, Fok JY, *et al*. Clinical and biological significance of tissue transglutaminase in ovarian carcinoma. *Cancer Res* 2008;68:5849–58.

12 Jeong J-H, Cho BC, Shim HS, *et al*. Transglutaminase 2 expression predicts progression free survival in non-small cell lung cancer patients treated with epidermal growth factor receptor tyrosine kinase inhibitor. *J Korean Med Sci* 2013;28:1005–14.

13 Condello S, Cao L, Matei D. Tissue transglutaminase regulates β-catenin signaling through a c-Src-dependent mechanism. *Faseb J* 2013;27:3100–12.

14 Lee J, Yakubov B, Ivan C, *et al*. Tissue transglutaminase activates cancer-associated fibroblasts and contributes to gemcitabine resistance in pancreatic cancer. *Neoplasia* 2016;18:689–98.

15 Kumar A, Gao H, Xu J, *et al*. Evidence that aberrant expression of tissue transglutaminase promotes stem cell characteristics in mammary epithelial cells. *PLoS One* 2011;6:e20701.

16 Kumar A, Xu J, Brady S, *et al*. Tissue transglutaminase promotes drug resistance and invasion by inducing mesenchymal transition in mammary epithelial cells. *PLoS One* 2010;5:e13390.

17 Kumar A, Xu J, Sung B, *et al*. Evidence that GTP-binding domain but not catalytic domain of transglutaminase 2 is essential for epithelial-to-mesenchymal transition in mammary epithelial cells. *Breast Cancer Res* 2012;14:R4.

18 Mehta K, Lopez-Berestein G, Moore WT, *et al*. Interferon-gamma requires serum retinoids to promote the expression of tissue transglutaminase in cultured human blood monocytes. *J Immunol* 1985;134:2053–6.

19 Cao L, Petrusca DN, Satpathy M, *et al*. Tissue transglutaminase protects epithelial ovarian cancer cells from cisplatin-induced apoptosis by promoting cell survival signaling. *Carcinogenesis* 2008;29:1893–900.

20 Mann AP, Verma A, Sethi G, *et al*. Overexpression of tissue transglutaminase leads to constitutive activation of nuclear factor-kappaB in cancer cells: delineation of a novel pathway. *Cancer Res* 2006;66:8788–95.

21 Mehta K, Fok J, Miller FR, *et al*. Prognostic significance of tissue transglutaminase in drug resistant and metastatic breast cancer. *Clin Cancer Res* 2004;10:8068–76.

22 Cao L, Shao M, Schilder J, *et al*. Tissue transglutaminase links TGF-β, epithelial to mesenchymal transition and a stem cell phenotype in ovarian cancer. *Oncogene* 2012;31:2521–34.

23 Kerr C, Szmacinski H, Fisher ML, *et al*. Transamidase site-targeted agents alter the conformation of the transglutaminase cancer stem cell survival protein to reduce GTP binding activity and cancer stem cell survival. *Oncogene* 2017;36:2981–90.

24 Sullivan KE, Rojas K, Cerione RA, *et al*. The stem cell/cancer stem cell marker ALDH1A3 regulates the expression of the survival factor tissue transglutaminase, in mesenchymal glioma stem cells. *Oncotarget* 2017;8:22325–43.

25 Szondy Z, Sarang Z, Molnar P. Transglutaminase 2-/- mice reveal a phagocytosis-associated crosstalk between macrophages and apoptotic cells 2003;100:7812–7.

26 Palucci I, Matic I, Falasca L. Transglutaminase type 2 plays a key role in the pathogenesis of Mycobacterium tuberculosis infection 2018;283:303–13.

27 Kim JH, Jeong EM, Jeong YJ. Transglutaminase 2 on the surface of dendritic cells is proposed to be involved in dendritic cell-T cell interaction 2014;289:55–62.

28 Kim JH, Hong JM, Jeong EM. Lack of transglutaminase 2 diminished T-cell responses in mice 2014;142:506–16.

29 Tóth B, Garabuczi E, Sarang Z, *et al*. Transglutaminase 2 is needed for the formation of an efficient phagocyte portal in macrophages engulfing apoptotic cells. *J Immunol* 2009;182:2084–92.

30 Falasca L, Iadevaia V, Ciccosanti F, *et al*. Transglutaminase type II is a key element in the regulation of the anti-inflammatory response elicited by apoptotic cell engulfment. *J Immunol* 2005;174:7330–40.

31 Sarang Z, Köröskényi K, Pallai A, *et al*. Transglutaminase 2 null macrophages respond to lipopolysaccharide stimulation by elevated proinflammatory cytokine production due to an enhanced αvβ3 integrin-induced Src tyrosine kinase signaling. *Immunol Lett* 2011;138:71–8.

32 Nanda N, Iismaa SE, Owens WA, *et al*. Targeted inactivation of Gh/tissue transglutaminase II. *J Biol Chem* 2001;276:20673–8.

33 Wang L, Fan J, Thompson LF, *et al*. CD73 has distinct roles in nonhematopoietic and hematopoietic cells to promote tumor growth in mice. *J Clin Invest* 2011;121:2371–82.

34 Chen S, Fan J, Zhang M, *et al*. CD73 expression on effector T cells sustained by TGF-β facilitates tumor resistance to anti-4-1BB/CD137 therapy. *Nat Commun* 2019;10:150.

35 Krutzik PO, Nolan GP. Intracellular phospho-protein staining techniques for flow cytometry: monitoring single cell signaling events. *Cytometry A* 2003;55:61–70.

36 Robinson MD, McCarthy DJ, Smyth GK. edgeR: a Bioconductor package for differential expression analysis of digital gene expression data. *Bioinformatics* 2010;26:139–40.

37 Chen EY, Tan CM, Kou Y, *et al*. Enrichr: interactive and collaborative HTML5 gene list enrichment analysis tool. *BMC Bioinformatics* 2013;14:128.

38 Kuleshov MV, Jones MR, Rouillard AD, *et al*. Enrichr: a comprehensive gene set enrichment analysis web server 2016 update. *Nucleic Acids Res* 2016;44:W90–7.

39 Roby KF, Taylor CC, Sweetwood JP, *et al*. Development of a syngeneic mouse model for events related to ovarian cancer. *Carcinogenesis* 2000;21:585–91.

40 Overacre-Delgoffe AE, Chikina M, Dadey RE, *et al*. Interferon-γ Drives T_{reg} Fragility to Promote Anti-tumor Immunity. *Cell* 2017;169:1130–41.

41 Raber PL, Thevenot P, Sierra R. Subpopulations of myeloid-derived suppressor cells impair T cell responses through independent nitric oxide-related pathways 2014;134:2853–64.

42 Juneja VR, McGuire KA, Manguso RT. PD-L1 on tumor cells is sufficient for immune evasion in immunogenic tumors and inhibits CD8 T cell cytotoxicity 2017;214:895–904.

43 Schmiedel BJ, Singh D, Madrigal A, *et al*. Impact of genetic polymorphisms on human immune cell gene expression. *Cell* 2018;175:1701–15.

44 Li B, Antonyak MA, Druso JE, *et al*. EGF potentiated oncogenesis requires a tissue transglutaminase-dependent signaling pathway leading to Src activation. *Proc Natl Acad Sci U S A* 2010;107:1408–13.

45 O'Shea JJ, Plenge R. Jak and STAT signaling molecules in immunoregulation and immune-mediated disease. *Immunity* 2012;36:542–50.

46 Zhu Y, Ju S, Chen E, *et al*. T-bet and eomesodermin are required for T cell-mediated antitumor immune responses. *J Immunol* 2010;185:3174–83.

47 Tai T-S, Pai S-Y, Ho I-C. GATA-3 regulates the homeostasis and activation of CD8+ T cells. *J Immunol* 2013;190:428–37.

48 Clouthier CM, Mironov GG, Okhonin V, *et al*. Real-time monitoring of protein conformational dynamics in solution using kinetic capillary electrophoresis. *Angew Chem Int Ed Engl* 2012;51:12464–8.

49 Yuan L, Siegel M, Choi K, *et al*. Transglutaminase 2 inhibitor, KCC009, disrupts fibronectin assembly in the extracellular matrix and sensitizes orthotopic glioblastomas to chemotherapy. *Oncogene* 2007;26:2563–73.

50 Herman JF, Mangala LS, Mehta K. Implications of increased tissue transglutaminase (TG2) expression in drug-resistant breast cancer (MCF-7) cells. *Oncogene* 2006;25:3049–58.

51 Mangala LS, Fok JY, Zorrilla-Calancha IR, *et al*. Tissue transglutaminase expression promotes cell attachment, invasion and survival in breast cancer cells. *Oncogene* 2007;26:2459–70.

52 Condello S, Sima L, Ivan C, *et al*. Tissue transglutaminase regulates interactions between ovarian cancer stem cells and the tumor niche. *Cancer Res* 2018;78:2990–3001.

53 Jones RA, Kotsakis P, Johnson TS, *et al*. Matrix changes induced by transglutaminase 2 lead to inhibition of angiogenesis and tumor growth. *Cell Death Differ* 2006;13:1442–53.

54 Xu L, Begum S, Hearn JD, *et al*. Gpr56, an atypical G protein-coupled receptor, binds tissue transglutaminase, TG2, and inhibits melanoma tumor growth and metastasis. *Proc Natl Acad Sci U S A* 2006;103:9023–8.

55 Bachmann MF, Wolint P, Schwarz K. Functional properties and lineage relationship of CD8+ T cell subsets identified by expression of IL-7 receptor alpha and CD62L 2005;175:4686–96.

56 Dalal V, Kumar R, Kumar S, *et al*. Biomarker potential of IL-6 and VEGF-A in ascitic fluid of epithelial ovarian cancer patients. *Clinica Chimica Acta* 2018;482:27–32.

57 Hotson AN, Hardy JW, Hale MB, *et al*. The T cell STAT signaling network is reprogrammed within hours of bacteremia via secondary signals. *J Immunol* 2009;182:7558–68.

58 Yu H, Pardoll D, Jove R. STATs in cancer inflammation and immunity: a leading role for STAT3. *Nat Rev Cancer* 2009;9:798–809.

59 Kortylewski M, Kujawski M, Wang T, *et al*. Inhibiting Stat3 signaling in the hematopoietic system elicits multicomponent antitumor immunity. *Nat Med* 2005;11:1314–21.

60 Ho HH, Ivashkiv LB. Role of STAT3 in type I interferon responses. Negative regulation of STAT1-dependent inflammatory gene activation. *J Biol Chem* 2006;281:14111–8.

61 Kujawski M, Zhang C, Herrmann A, *et al*. Targeting STAT3 in adoptively transferred T cells promotes their in vivo expansion and antitumor effects. *Cancer Res* 2010;70:9599–610.

62 Yue C, Shen S, Deng J, *et al*. STAT3 in CD8+ T cells inhibits their tumor accumulation by downregulating CXCR3/CXCL10 axis. *Cancer Immunol Res* 2015;3:864–70.

63 Yue C, Shen S, Deng J, *et al*. STAT3 in CD8^{+} T Cells Inhibits Their Tumor Accumulation by Downregulating CXCR3/CXCL10 Axis. *Cancer Immunol Res* 2015;3:864–70.

64 Cheng F, Wang H-W, Cuenca A, *et al*. A critical role for STAT3 signaling in immune tolerance. *Immunity* 2003;19:425–36.

65 Kortylewski M, Xin H, Kujawski M, *et al*. Regulation of the IL-23 and IL-12 balance by STAT3 signaling in the tumor microenvironment. *Cancer Cell* 2009;15:114–23.

66 Cui W, Liu Y, Weinstein JS, *et al*. An interleukin-21-interleukin-10-STAT3 pathway is critical for functional maturation of memory CD8+ T cells. *Immunity* 2011;35:792–805.

67 Zhang H, Chen Z, Miranda RN, *et al*. Tg2 and NF-κB signaling coordinates the survival of mantle cell lymphoma cells via IL6-Mediated autophagy. *Cancer Res* 2016;76:6410–23.

68 Huang B, Song B-L, Xu C. Cholesterol metabolism in cancer: mechanisms and therapeutic opportunities. *Nat Metab* 2020;2:132–41.

69 He M, Zhang W, Dong Y, *et al*. Pro-Inflammation NF-κB signaling triggers a positive feedback via enhancing cholesterol accumulation in liver cancer cells. *J Exp Clin Cancer Res* 2017;36:15.

70 Martinez FO, Helming L, Milde R, *et al*. Genetic programs expressed in resting and IL-4 alternatively activated mouse and human macrophages: similarities and differences. *Blood* 2013;121:e57–69.

71 Lin H, Wei S, Hurt EM. Host expression of PD-L1 determines efficacy of PD-L1 pathway blockade-mediated tumor regression 2018;128:805–15.